Advanced mechanics

Vincent Démery

February 25, 2021

Contents

Contents **4**

1 Solid mechanics **5**

1.1 Stress and strain on a simple example . . . 5
1.2 Strain and stress tensors, Hooke's law . . . 5
1.3 Equilibrium . . . 6

2 Euler-Bernouilli beam theory and applications **7**

2.1 Two dimensional elasticity with plane strain or plane stress . . . 7
2.1.1 Plane stress . . . 7
2.1.2 Plane strain . . . 7
2.2 Flexion of a rod . . . 7
2.3 Equilibrium equations of a rod . . . 9
2.4 Euler buckling . . . 10
2.4.1 Stability analysis at imposed force . . . 10
2.4.2 Scaling analysis at imposed deformation . . . 10
2.5 Bending of plates . . . 11
2.6 Buckling on a foundation, wrinkling, folding . . . 11
2.6.1 Wrinkling . . . 11
2.6.2 Non-linearities, folding . . . 13
2.7 Elasto-capillary phenomena . . . 14

3 Rods **15**

3.1 Geometry . . . 15
3.2 Twist of a rod . . . 15
3.3 Energy and equilibrium equations . . . 17
3.4 Invariants . . . 17
3.5 Localized helix . . . 18

4 Sheets **21**

4.1 Geometry and mechanics of sheets . . . 21

4.1.1 Stretching and bending moduli . . . 21
4.1.2 Gauss theorema egregium . . . 21
4.1.3 Föppl-von Kármán equations . . . 23
4.1.4 Reduced models . . . 24
4.1.5 Numerical simulations . . . 26
4.2 Instabilities, pattern formation . . . 27
4.2.1 Wrinkles . . . 27
4.2.2 Cascades . . . 31
4.2.3 Crumples and folds . . . 32
4.3 Crumpled sheets . . . 33
4.3.1 Conical singularities . . . 33
4.3.2 Ridge singularities . . . 35
4.3.3 Experimental and numerical studies . . . 36

Bibliography **39**

Chapter 1

Solid mechanics

Here we recall the main equations of solid mechanics.

1.1 Stress and strain on a simple example

As a simple example, we consider a piece of rubber stretched by a force F in the x-direction, and free in the y and z directions. Under this force, the length of this piece extends from length L to length $L + \Delta L$. We denote the strain in the x-direction

$$\epsilon_x = \frac{\Delta L}{L}. \tag{1.1}$$

The force is actually proportional to the area A of the cross-section in the (y, z) plane, and, in the linear regime of the material to the strain ϵ_x and to the Young's modulus E of the material:

$$F = EA\epsilon_x. \tag{1.2}$$

The force per unit area is the *stress*

$$\sigma_x = \frac{F}{A} = E\epsilon_x. \tag{1.3}$$

In the transverse directions y and z, there is no stress ($\sigma_y = \sigma_z = 0$) but we can observe a contraction, which is proportional to the longitudinal stress:

$$\epsilon_y = \epsilon_z = -\frac{\nu}{E}\sigma_x, \tag{1.4}$$

where ν is the Poisson ratio of the material.

The Young's modulus E and Poisson ratio ν characterize any isotropic material. The above equations contain all we need to know to handle general deformations, we just have to make them local and tensorial, as we will see.

1.2 Strain and stress tensors, Hooke's law

First, we have to define the strain. We have given a macroscopic definition in Eq. (1.1), but we need a microscopic, or local, one. We denote $u(x)$ the longitudinal displacement of a piece of material at position x. Setting $u(0) = 0$, we should have $u(L) = \Delta L$, and a regular deformation imposes

$u(x) = \frac{\Delta L}{L} x$. The strain can then be obtained locally as $\epsilon_x = \partial_x u$. In general, the displacement is a vector field $\boldsymbol{u}(\boldsymbol{r})$, and its derivative generalizes to a rank 2 tensor:

$$\epsilon_{ij} = \frac{1}{2} \left(\partial_i u_j + \partial_j u_i \right). \tag{1.5}$$

We took it to be symmetric for a reason that will become clear below.

Alternatively, the strain can be derived from the metric. Consider a deformation that takes a piece of material from $\boldsymbol{r}$ to $\boldsymbol{R}(\boldsymbol{r}) = \boldsymbol{r} + \boldsymbol{u}(\boldsymbol{r})$. Assuming that the material is initially at rest, its reference metric is $g^0_{ij} = \delta_{ij}$. Now the metric of the deformed material is

$$g_{ij} = \partial_i \boldsymbol{R} \cdot \partial_j \boldsymbol{R}. \tag{1.6}$$

To order one in $\nabla \boldsymbol{u}$, the metric is

$$g_{ij} = \delta_{ij} + \partial_i u_j + \partial_j u_i. \tag{1.7}$$

The strain is defined as the difference with the reference metric:

$$\epsilon_{ij} = \frac{g_{ij} - g^0_{ij}}{2}. \tag{1.8}$$

Since the metric is symmetric, ϵ_{ij} should be symmetric.

The stress describes the forces in the material. It is also a rank 2 tensor, which we denote σ_{ij}. The force exerted through a surface of a normal $\boldsymbol{n}$ and area δA is given by

$$\delta F_i = \delta A \sigma_{ij} n_j. \tag{1.9}$$

We use Einstein convention for the summation over repeated indices. From a simple calculation of the moment of the forces exerted on a small cube, one can show that the stress tensor is symmetric.

The only isotropic tensorial relation compatible with the relations of Sec. 1.1 is the Hooke's law:

$$\boxed{\sigma_{ij} = \frac{E}{1+\nu} \left(\epsilon_{ij} + \frac{\nu}{1-2\nu} \epsilon_{kk} \delta_{ij} \right).} \tag{1.10}$$

This relation can be inverted; taking the trace of this relation we get $\sigma_{kk} = \frac{E}{1-2\nu} \epsilon_{kk}$, and we deduce

$$\boxed{\epsilon_{ij} = \frac{1}{E} \left[(1+\nu) \sigma_{ij} - \nu \sigma_{kk} \delta_{ij} \right].} \tag{1.11}$$

In the example of Sec. 1.1, the only non zero component of the stress field is σ_{xx}. From the inverse of Hooke's law, we get for the strain:

$$\epsilon = \frac{\sigma_{xx}}{E} \begin{pmatrix} 1 & 0 & 0 \\ 0 & -\nu & 0 \\ 0 & 0 & -\nu \end{pmatrix}. \tag{1.12}$$

1.3 Equilibrium

From a force balance on a small volume element, we arrive at the equilibrium equation:

$$\boxed{\partial_i \sigma_{ij} = 0.} \tag{1.13}$$

By computing the work of the forces on a small volume element, we find the volumic energy density:

$$\boxed{e = \frac{1}{2} \sigma_{ij} \epsilon_{ij}.} \tag{1.14}$$

Chapter 2

Euler-Bernouilli beam theory and applications

References: [Audoly and Pomeau, 2010, Chap. 3.3].

In this chapter we present the Euler-Bernouilli theory for inextensible beams (or rods), and application to Euler buckling of rods and plates, and to wrinkling on a foundation.

2.1 Two dimensional elasticity with plane strain or plane stress

2.1.1 Plane stress

The Euler-Bernouilli (EB) beam theory can be considered as a two-dimensional theory, meaning that the stresses in third dimension z are zero: $\sigma_{iz} = 0$. This is the plane stresses assumption.

Using $\sigma_{zz} = 0$ in the Hooke's law (1.10), we get $\epsilon_{zz} = -\frac{\nu}{1-\nu}(\epsilon_{xx}+\epsilon_{yy})$, so that $\epsilon_{kk} = \frac{1-2\nu}{1-\nu}(\epsilon_{xx}+\epsilon_{yy})$. Defining

$$\epsilon^{(2)}_{kk} = \epsilon_{xx} + \epsilon_{yy}, \tag{2.1}$$

the Hooke's law becomes:

$$\boxed{\sigma_{ij} = \frac{E}{1+\nu}\left(\epsilon_{ij} + \frac{\nu}{1-\nu}\epsilon^{(2)}_{kk}\delta_{ij}\right).} \tag{2.2}$$

Now we do not have to consider the stress and strain in the z direction.

2.1.2 Plane strain

In case of plane strain, which should be used for plates that are "large" in the z direction, $\epsilon_{iz} = 0$.

Using the condition $\epsilon_{zz} = 0$ in the inverse of Hooke's law (Eq. (1.11)), we get $\sigma_{zz} = \nu\sigma^{(2)}_{kk}$.

2.2 Flexion of a rod

Here we compute the bending energy of a rod. We consider a rod bent in the (x, y) plane with a radius of curvature R (Fig. 2.1).

Before going through the complete calculation we use scaling arguments. The energy per unit length of a rod with curvature $\kappa = R^{-1}$ should be quadratic in κ: $U \sim B\kappa^2$, where B is the bending

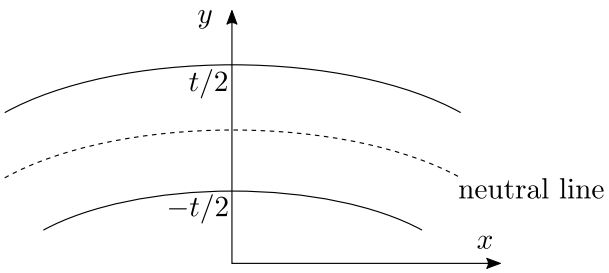

Figure 2.1: Rod bent in one direction.

modulus. Dimensionnally, $[B] = EL$ (energy × length). The bending modulus should depend on the Young's modulus E of the material and the transverse lengthscale of the rod t. Since $[E] = EL^{-3}$, we should have $B \sim Et^4$.

On the sides of the rod, the boundary conditions for the stress are $\sigma_{xy} = \sigma_{yy} = 0$. We therefore assume that these stresses are zero so that only σ_{xx} is not zero. These relations imply that $\epsilon_{xy} = 0$ and $\epsilon_{yy} + \frac{\nu}{1-\nu}\epsilon^{(2)}_{kk} = 0$, leading to $\epsilon_{yy} = -\nu\epsilon_{xx}$.

The main deformation is the extension of the lines on "the long side" of the rod (above the neutral line on Fig. 2.1) and the compression of the lines on "the short side" (below the neutral line). Consider a line of length δx in the longitudinal direction in the rod at rest, at a height Δy above the neutral line (we can have $\Delta y < 0$). In the bent rod, this line takes the length $\delta x' = \delta x \times \frac{R+\Delta y}{R}$, so that the elongation is

$$\epsilon_{xx} = \frac{\delta x' - \delta x}{\delta x} = \frac{\Delta y}{R} = \frac{y - y_0}{R}, \tag{2.3}$$

where y_0 is the height of the neutral line.

The stress field is given by $\sigma_{xx} = E\epsilon_{xx}$; it satisfies the equilibrium equation $\partial_i \sigma_{ix} = \partial_x \sigma_{xx} = 0$.

We can integrate the stress field to get the displacement field:

$$\epsilon_{xx} = \partial_x u_x = \frac{y - y_0}{R}, \tag{2.4}$$

$$\epsilon_{xy} = \frac{1}{2}\left(\partial_x u_y + \partial_y u_x\right) = 0, \tag{2.5}$$

$$\epsilon_{yy} = \partial_y u_y = -\nu\frac{y - y_0}{R}. \tag{2.6}$$

We get

$$u_x = \frac{x(y - y_0)}{R}, \tag{2.7}$$

$$u_y = -\frac{x^2}{2R} - \nu\frac{(y - y_0)^2}{R}. \tag{2.8}$$

The first term in u_y is just the conformation to a circle with radius R.

From the stress and strain we can compute the energy. The volumic energy is

$$e = \frac{1}{2}\sigma_{ij}\epsilon_{ij} = \frac{1}{2}\sigma_{xx}\epsilon_{xx} = \frac{E}{2}\epsilon^2_{xx} = \frac{E(y - y_0)^2}{2R^2}. \tag{2.9}$$

The energy per unit length U/L is obtained by integrating over a cross-section $\mathcal{S}$:

$$\frac{U}{L} = \frac{E}{2R^2}\int_{\mathcal{S}} (y - y_0)^2 \mathrm{d}y\mathrm{d}z. \tag{2.10}$$

The neutral line has to be chosen in order to minimize the energy: $\partial_{y_0} U = 0$, which leads to

$$\boxed{y_0 = \frac{\int_{\mathcal{S}} y \mathrm{d}y\mathrm{d}z}{\int_{\mathcal{S}} \mathrm{d}y\mathrm{d}z} = \frac{1}{S}\int_{\mathcal{S}} y\mathrm{d}y\mathrm{d}z = \langle y \rangle_{\mathcal{S}}.} \tag{2.11}$$

Here, S is the area of the cross-section and $\langle\cdot\rangle_{\mathcal{S}}$ denotes the average over the cross-section. $\langle y\rangle_{\mathcal{S}}$ is the position of the "center of mass" of the cross-section. The bending modulus is then defined as

$$\boxed{B = E\int_{\mathcal{S}} (y-y_0)^2 \mathrm{d}y\mathrm{d}z = ES\langle (y-y_0)^2\rangle_{\mathcal{S}},} \tag{2.12}$$

so that

$$\frac{U}{L} = \frac{B}{2R^2}. \tag{2.13}$$

We can compute the moment along $\hat{\boldsymbol{e}}_z$ exerted "through a cross-section" (we mean the moment exerted by the right part of the rod on the left part):

$$M = -\int_{\mathcal{S}} y\sigma_{xx}\mathrm{d}y\mathrm{d}z = -\frac{E}{R}\int_{\mathcal{S}} y(y-y_0)\mathrm{d}y\mathrm{d}z = -\frac{ES}{R}\langle y(y-y_0)\rangle_{\mathcal{S}} = -\frac{B}{R}. \tag{2.14}$$

Note that this form of the moment is expected from the energy above.

If the cross-section is rectangular, with height (along y) t and width (along z) w, its bending modulus is

$$B = \frac{Et^3 w}{12}. \tag{2.15}$$

If the cross-section is a disk with radius r, the bending modulus is

$$B = \frac{\pi E r^4}{4}. \tag{2.16}$$

2.3 Equilibrium equations of a rod

Now assume that the (centre line of the) rod describes a curve in the (x, y) plane. We denote s the curvilinear coordinate along the rod, $\boldsymbol{t}(s)$ the unit vector tangent to the rod at s and $\theta(s)$ the angle between $\boldsymbol{e}_x$ and $\boldsymbol{t}(s)$.

The local curvature is given by $R(s)^{-1} = |\theta'(s)|$, hence from Eq. (2.13) the bending energy of the rod is

$$\boxed{U = \frac{B}{2}\int \theta'(s)^2 \mathrm{d}s.} \tag{2.17}$$

The moment exerted through the cross-section at s (by the rod parts with coordinates $s' > s$ on the rod parts where $s' < s$) is, from Eq. (2.14),

$$\boxed{M(s) = B\theta'(s).} \tag{2.18}$$

Note that $\theta'(s) < 0$ in Fig. 2.1.

A force $\boldsymbol{F}(s)$ (the "vectorial tension") can be exerted through the cross-section at s. With the coordinates on Fig. 2.1, the force is $F_i = \int \sigma_{ix}\mathrm{d}y\mathrm{d}z$. Note that a force that is not along $\boldsymbol{t}(s)$ requires a $\sigma_{xy} \neq 0$, which has not been considered in the equation for the bending modulus. A balance of moments on the section $[s, s+\delta s]$ of the rod gives

$$-M(s) + \boldsymbol{t}(s)\delta s \times \boldsymbol{F}(s) + M(s+\delta s) = 0, \tag{2.19}$$

from which we deduce

$$\boxed{M'(s) + \boldsymbol{t}(s) \times \boldsymbol{F}(s) = 0.} \tag{2.20}$$

The projection on $\hat{\boldsymbol{e}}_z$ is assumed.

If a force per unit length $\boldsymbol{f}(s)$ is exerted on the rod, then the vectorial tension obeys

$$\boxed{\boldsymbol{F}'(s) + \boldsymbol{f}(s) = 0.} \tag{2.21}$$

2.4 Euler buckling

2.4.1 Stability analysis at imposed force

We consider a rod of length L along $\hat{\boldsymbol{e}}_x$ submitted to a compressive force F. We assume that its ends are free to rotate but can only move in the x direction. We show that there is a threshold force F_c above which the rod *buckles* and adopts a curved shape.

From dimensional arguments, the critical force can only depend on the length L and the bending modulus B of the rod, so that we should have $F_c \sim B/L^2$.

We look at the minimal value of F for a buckled solution to exist. We assume a small departure from the straight line, so that the angle $\theta(s)$ between $\hat{\boldsymbol{e}}_x$ and $\boldsymbol{t}(s)$ is small ($\theta(s) \ll 1$). The moment transmitted along the rod is $M(s) = B\theta'(s)$ (Eq. (2.18)). The boundary condition is $M(0) = M(L) = 0$, and the moment evolves according to Eq. (2.20):

$$M'(s) = -([\cos(\theta)\hat{\boldsymbol{e}}_x + \sin(\theta)\hat{\boldsymbol{e}}_y] \times [-F\hat{\boldsymbol{e}}_x]) \cdot \hat{\boldsymbol{e}}_z = -F\sin(\theta(s)) \simeq -F\theta(s). \tag{2.22}$$

We thus get a closed equation for $\theta(s)$:

$$\theta''(s) = -\frac{F}{B}\theta(s). \tag{2.23}$$

This equation is solved by $\theta(s) = \cos(ks)$ if $k = \sqrt{\frac{F}{B}} = \frac{\pi n}{L}$, where n is an integer. The smallest force for which there is a solution corresponds to $n = 1$:

$$\boxed{F_c = \frac{\pi^2 B}{L^2}.} \tag{2.24}$$

2.4.2 Scaling analysis at imposed deformation

Here we assume that the rod is compressed by a length ΔL, corresponding to a compressive strain $\epsilon = \Delta L/L$. The elastic energy per unit length of the compressed rod is

$$U_{\text{comp}} \sim Y\epsilon^2, \tag{2.25}$$

where $Y = Et^2$ is the stretching modulus of the rod. The compressive force associated to a compression ϵ is $F = Y\epsilon$.

We want to estimate the energy of a buckled rod, where the "compression" ϵ is accomodated by buckling instead of compression of the material. The vertical displacement H of the center of the rod should satisfy

$$\epsilon \sim \frac{H^2}{L^2} \tag{2.26}$$

(the arclength of a segment of a curve $h(x)$ is given by $\sqrt{1+h'(x)^2}\delta x \simeq (1+\frac{1}{2}h'(x)^2)\delta x$ if $|h'(x)| \ll 1$, and here $h' \sim H/L$). The curvature is $R^{-1} = h''(x) \sim H/L^2$. The bending energy per unit length is thus

$$U_{\text{bend}} \sim \frac{B}{R^2} \sim \frac{BH^2}{L^4} \sim \frac{B\epsilon}{L^2}. \tag{2.27}$$

The bending energy is smaller than the stretching energy for

$$\boxed{\epsilon > \epsilon_{\text{c}} \sim \frac{B}{YL^2} \sim \frac{t^2}{L^2},} \tag{2.28}$$

which corresponds to a compressive force $F_{\text{c}} \sim Y\epsilon_{\text{c}} \sim B/L^2$.

Another way to arrive at the result is to say that a compressive force F corresponds to the energy $U_{\text{comp}} = -F\epsilon$, which should be compared to U_{bend}.

Note that the critical displacement is $\Delta L_{\text{c}} = L\epsilon_{\text{c}} \sim t^2/L \ll t$: it is much smaller than the thickness of the rod. For a sheet of paper, $L \sim 30\,\text{cm}$, $t \sim 100\,\mu\text{m}$, we get $\Delta L_{\text{c}} \sim 30\,\text{nm}$! This separation of length scales ($\Delta L_{\text{c}} \ll L$) supports the inextensible rod model.

2.5 Bending of plates

Here we should use a plane strain condition, $\epsilon_{iz} = 0$. Indeed using a plane stress condition leads to $\epsilon_{zz} = -\nu\epsilon_{xx} = \epsilon_{yy} = -\nu\frac{y-y_0}{R} = \partial_z u_z$. This requires a strain of the form $u_z = -\nu z\frac{y-y_0}{R}$, which may be large for a wide sheet.

We adapt the calculation of Sec. 2.2 with this condition. We get the same elongation

$$\epsilon_{xx} = \frac{\Delta y}{R} = \frac{y-y_0}{R}. \tag{2.29}$$

From $\sigma_{yy} = 0$ and Hooke's law with $\epsilon_{zz} = 0$, we get $\epsilon_{yy} = -\frac{\nu}{1-\nu}\epsilon_{xx}$. Then Hooke's law gives

$$\sigma_{xx} = \frac{E}{1-\nu^2}\epsilon_{xx}, \tag{2.30}$$

hence the volumic energy is now

$$e = \frac{E(y-y_0)^2}{2(1-\nu^2)R^2}. \tag{2.31}$$

The difference with the previous calculation is just this factor $1/(1-\nu^2)$ in the energy.

Using the bending modulus of a rectangular rod (Eq. (2.15)), we get the bending modulus *per unit width* of a sheet of thickness t:

$$\boxed{B = \frac{Et^3}{12(1-\nu^2)}.} \tag{2.32}$$

2.6 Buckling on a foundation, wrinkling, folding

2.6.1 Wrinkling

2.6.1.1 Energetic approach

We consider the buckling of a compressed film lying on top of a liquid (typically at a water-air interface). Upon buckling, fluid has to be displaced, which costs gravitational energy. As a consequence, the

"wavelength" is not set by the length of the film, as with Euler buckling, but by a competition of bending and gravity, leading to a wrinkle pattern, which we characterize here.

A simple wrinkle pattern (with parallel and regular wrinkles) is characterized by the amplitude A of the wrinkles and their wavelength λ. The typical curvature is $R^{-1} \sim A/\lambda^2$, so that the bending energy per unit area is

$$U_{\text{bend}} \sim \frac{BA^2}{\lambda^4}, \tag{2.33}$$

On the other hand, it takes gravitational energy to displace liquid:

$$U_{\text{grav}} \sim \rho g A^2, \tag{2.34}$$

where ρ is the density difference between the two phases (below and above the sheet) and g is the gravitational acceleration. The compression is

$$\epsilon \sim \frac{A^2}{\lambda^2}. \tag{2.35}$$

First, we assume that the compression is imposed: Eq. (2.35) is a slaving condition between the amplitude and the wavelength. Cancelling the amplitude in the energies, we get $U_{\text{bend}} \sim B\epsilon/\lambda^2$, and $U_{\text{grav}} \sim \rho g \epsilon \lambda^2$. The total energy is minimal when these two energies are comparable, leading to

$$\boxed{\lambda \sim \left(\frac{B}{\rho g}\right)^{1/4}.} \tag{2.36}$$

Note that the wavelength does not depend on the compression. This length may be refered to as the bendo-gravity length. The corresponding energy is

$$\boxed{U_{\text{bendo-grav}} \sim \epsilon\sqrt{B\rho g}.} \tag{2.37}$$

This analysis is very common to determine how the wavelength depends on the parameters of the problem. Small wavelengths are usually penalized by the bending energy. On the contrary, many mechanisms can penalize large amplitudes, and thus large wavelengths via the slaving condition (2.35); they lead to the energy $U \sim KA^2$, where K is the "effective substrate stiffness". The origin can be gravity, elasticity of the substrate [Brau et al., 2011], or two-dimensional effects discussed in Sec. 4.2.1.2: tension or curvature in the transverse direction [Cerda and Mahadevan, 2003, Paulsen et al., 2016]. The resulting wavelength is thus

$$\lambda \sim \left(\frac{B}{K}\right)^{1/4}. \tag{2.38}$$

If we assume a compressive stress σ (we take $\sigma > 0$ for a compressive stress here), with an additional energy

$$U_{\text{comp}} \sim -\sigma\epsilon. \tag{2.39}$$

Wrinkles are favored when

$$\sigma > \sigma_c \sim \sqrt{B\rho g}. \tag{2.40}$$

This is just Euler buckling with a characteristic length set by λ instead of L.

2.6.1.2 Stability analysis

We can go beyond scaling analysis to get the buckling threshold. If the height of the film is given by $h(x)$, to lowest order in h the energy is given by

$$U = \frac{1}{2}\int \left[Bh''(x)^2 + \rho g h(x)^2 - \sigma h'(x)^2\right] \mathrm{d}x. \tag{2.41}$$

The corresponding Euler-Lagrange equation is

$$Bh^{(4)}(x) + \sigma h''(x) + \rho g h(x) = 0. \tag{2.42}$$

We look for a harmonic solution, $h(x) = A\cos(kx)$. The equation for k is

$$Bk^4 - \sigma k^2 + \rho g = 0. \tag{2.43}$$

It has a solution if $\sigma^2 - 4B\rho g > 0$, hence

$$\sigma_\mathrm{c} = 2\sqrt{B\rho g}. \tag{2.44}$$

The solution is

$$k^* = \left(\frac{\rho g}{B}\right)^{1/4}, \tag{2.45}$$

corresponding to the wavelength found above.

2.6.2 Non-linearities, folding

In experiments of elastic sheets or even granular layers [Vella et al., 2004] sitting on top of a liquid, soon after wrinkles form they give way to a more localized deformation: a fold [Pocivavsek et al., 2008].

This phenomenon can be undestood first from a simple scaling analysis. The total energy of the wrinkled state obtained upon compression of a sheet of length L by a length $\Delta = \epsilon L$ is (Eq. (2.37)):

$$U_\mathrm{wr} \sim \Delta\sqrt{B\rho g}. \tag{2.46}$$

On the other hand, an antisymmetric fold with two loops of size ℓ can take any amount of excess length with an energy $\ell[B\ell^{-2} + \rho g\ell^2]$ [Démery et al., 2014], leading to

$$U_\mathrm{fold} \sim \lambda\sqrt{B\rho g} \tag{2.47}$$

after optimizing over ℓ, where λ is the bendo-gravity length, Eq. (2.36). Forming a fold is thus energetically favorable for $\Delta > \lambda$, which occurs very quickly in long sheets.

To go beyond the scaling analysis, we can write the exact form of the energy associated to this problem. Denoting s the arclength along the sheet and $\phi(s)$ the angle between the sheet and an horizontal plane, the energy is

$$U = \frac{1}{2}\int \left[B\phi'(s)^2 + \rho g h(s)^2\cos(\phi(s))\right] \mathrm{d}s. \tag{2.48}$$

To be able to solve this problem using variational calculus, we should incorporate the relation between $h(s)$ and $\phi(s)$, $h'(s) = \sin(\phi(s))$, and the expression of the compressed length $\Delta = \int[1-\cos(\phi(s))]\mathrm{d}s$. The functional to minimize is thus

$$I[h,\phi] = \int \left[\frac{B}{2}\phi'(s)^2 + \frac{\rho g}{2}h(s)^2\cos(\phi(s)) - \sigma[1-\cos(\phi(s))] - Q(s)[h'(s) - \sin(\phi(s))]\right] \mathrm{d}s. \tag{2.49}$$

Expanding to order h^2 and ϕ^2, we recover the linear equations of the previous section. The lowest non-linear order is obtained by expanding up to h^4; there the solution minimizing the energy is a modulated sinusoïd, representing localization with a characteristic length that is infinite at the buckling threshold and decreases after the threshold [Audoly, 2011]. This problem also admits an exact solution [Diamant and Witten, 2011]:

$$\phi(s) = 4 \arctan\left(\frac{\kappa \sin(ks)}{k \cosh(\kappa s)}\right), \tag{2.50}$$

where $k = \sqrt{2+\sigma}/2$ and $\kappa = \sqrt{2-\sigma}/2$ in dimensionless form (lengths rescaled by λ and energies by $\lambda\sqrt{B\rho g}$). Close to the transition $\kappa \ll 1$, this is a modulated sinusoid and the width of the modulation is κ^{-1}.

When the film rests on a gel instead of a liquid, the non-linearities of the substrate lead to period doubling [Brau et al., 2011]. Note that here the buckling of the film is obtained by bending the gel-film system.

2.7 Elasto-capillary phenomena

When solids are in contact with liquid interfaces, the surface tension γ of the interface can deform the solid. The lengthscale emerging from comparing the surface tension with the elasticity of the solid, set by its Young's modulus E, is the elasto-capillary length

$$\ell_{\mathrm{EC}} = \frac{\gamma}{E}. \tag{2.51}$$

For an air-water interface $\gamma \simeq 72\,\mathrm{mN\,m^{-1}}$, and for a very soft gel $E \sim 1\,\mathrm{kPa}$, so that $\ell_{\mathrm{EC}} \sim 0.1\,\mathrm{mm}$. This is small but it can be observed easily [Style et al., 2013]. For stiffer solids the elasto-capillary length is in the nanometer range.

Liquid interfaces can instead easily deform slender bodies such as sheets. Assuming that the surface tension is too small to stretch the sheet ($\gamma \ll Y = Et$), the relevant lengthscale is the bendo-capillary length

$$\ell_{\mathrm{BC}} = \sqrt{\frac{B}{\gamma}} \sim \sqrt{\frac{t^3}{\ell_{\mathrm{EC}}}}. \tag{2.52}$$

This length is the typical radius of curvature that surface tension can generate; this also means that sheets longer than ℓ_{BC} can be bent, while sheets smaller than ℓ_{BC} cannot. Surface tension can thus be used to create three dimensional structures from flat sheets: this is the so-called "capillary origami" [Py et al., 2007]. In this example, $t \simeq 60\,\mu\mathrm{m}$, $E \sim 2$ MPa (PDMS), so that $\ell_{\mathrm{BC}} \sim 0.7$ mm.

More generally, surface tension is a convenient way to apply controlled loads to sheets to investigate their mechanical properties [Roman and Bico, 2010, Huang et al., 2007].

Chapter 3

Rods

3.1 Geometry

In this section we describe how to parametrize the geometry of an inextensible rod.

To each point of the centerline (the line that remains inextensible when the rod is deformed), identified by the curvilinear coordinate s, we attach the orthogonal material frame $(\boldsymbol{d}_i(s))_{1\leq i\leq 3}$. We take $\boldsymbol{d}_3(s)$ to be the vector tangent to the centerline: $\boldsymbol{d}_3(s) = \boldsymbol{R}'(s)$, where $\boldsymbol{R}(s)$ describes the position of the centerline. The other vectors $\boldsymbol{d}_1(s)$ and $\boldsymbol{d}_2(s)$ are in the plane of a cross-section.

The deformation of the rod is described by the evolution of this frame along the rod. The orthogonality of the frame, $\boldsymbol{d}_i(s) \cdot \boldsymbol{d}_j(s) = \delta_{i,j}$, imposes that

$$\boldsymbol{d}_i' \cdot \boldsymbol{d}_i = 0, \tag{3.1}$$

$$\boldsymbol{d}_i' \cdot \boldsymbol{d}_j = -\boldsymbol{d}_i \cdot \boldsymbol{d}_j'. \tag{3.2}$$

Hence there exists functions $\kappa^{(1)}(s)$, $\kappa^{(2)}(s)$ and $\tau(s)$ such that

$$\boldsymbol{d}_1' = \tau \boldsymbol{d}_2 - \kappa^{(2)} \boldsymbol{d}_3, \tag{3.3}$$

$$\boldsymbol{d}_2' = -\tau \boldsymbol{d}_1 + \kappa^{(1)} \boldsymbol{d}_3, \tag{3.4}$$

$$\boldsymbol{d}_3' = \kappa^{(2)} \boldsymbol{d}_1 - \kappa^{(1)} \boldsymbol{d}_2. \tag{3.5}$$

τ is the twist, $\kappa^{(i)}$ is the bending in the direction $i \in \{1, 2\}$. These equations can be rewritten by introducing the Darboux vector

$$\boxed{\boldsymbol{\Omega} = \kappa^{(1)} \boldsymbol{d}_1 + \kappa^{(2)} \boldsymbol{d}_2 + \tau \boldsymbol{d}_3;} \tag{3.6}$$

they become simply

$$\boxed{\boldsymbol{d}_i' = \boldsymbol{\Omega} \times \boldsymbol{d}_i.} \tag{3.7}$$

The material frame used here is not the same as the Serret-Frenet frame which is defined for a curve $\boldsymbol{R}(s)$ but does not distinguish the bending directions and does not consider the physical twist.

3.2 Twist of a rod

For a more detailed calculation see [Audoly and Pomeau, 2010, Sec. 3.4].

We consider a rod with a twist τ: the cross section rotates along the center-line with a "pulsation" τ with the curvilinear coordinate s. On dimensional grounds, we expect an energy per unit length $U/L \sim J\tau^2$, where $J \sim Et^4$.

We assume that the centerline is the z-axis (so that $s = z$) and use (x, y) as the material coordinates in the plane of the cross-section. Since there is an helicoidal symmetry, we only have to describe the deformation of the cross-section at $z = 0$. At order 1 in τ, it reduces to

$$\boldsymbol{R}(x, y, 0) = \begin{pmatrix} x \\ y \\ Z(x, y) \end{pmatrix}. \tag{3.8}$$

The displacements parallel to the cross section vanish at this order. The cross-section at z is then given by

$$\boldsymbol{R}(x, y, z) = \begin{pmatrix} x\cos(\tau z) - y\sin(\tau z) \\ y\cos(\tau z) + x\sin(\tau z) \\ z + Z(x, y) \end{pmatrix}. \tag{3.9}$$

The non-zero components of the strain field are

$$\epsilon_{xz} = \frac{1}{2}(\partial_x Z - \tau y), \tag{3.10}$$

$$\epsilon_{yz} = \frac{1}{2}(\partial_y Z + \tau x). \tag{3.11}$$

Since the strain tensor is traceless, it is proportional to the stress tensor:

$$\sigma_{ij} = \frac{E}{1+\nu}\epsilon_{ij}. \tag{3.12}$$

The equilibrium condition for the stress is $\partial_i \sigma_{ij} = 0$, hence for the strain $\partial_x \epsilon_{xz} + \partial_y \epsilon_{yz} = 0$, leading to

$$\nabla^2 Z = 0. \tag{3.13}$$

There is a stress free boundary condition, $n_i \sigma_{ij} = 0$ on the sides of the rod, where $\boldsymbol{n}$ is the normal to the edge of the rod. This gives a source term for $Z(x, y)$:

$$\boldsymbol{n} \cdot \nabla Z = \tau(\boldsymbol{n} \times \boldsymbol{r}) \cdot \boldsymbol{e}_z, \tag{3.14}$$

where $\boldsymbol{r} = (x, y)$. We indeed find that Z is proportional to τ. We can introduce normalized quantities $\bar{Z} = Z/\tau$, $\bar{\epsilon} = \epsilon/\tau$; they satisfy

$$\bar{\epsilon}_{xz} = \frac{1}{2}(\partial_x \bar{Z} - y), \tag{3.15}$$

$$\bar{\epsilon}_{yz} = \frac{1}{2}(\partial_y \bar{Z} + x), \tag{3.16}$$

$$\nabla^2 \bar{Z} = 0, \tag{3.17}$$

$$\boldsymbol{n} \cdot \nabla \bar{Z} = (\boldsymbol{n} \times \boldsymbol{r}) \cdot \boldsymbol{e}_z, \tag{3.18}$$

the last equation being satisfied on the boundary.

The twist energy (per unit length) is then given by

$$\frac{U}{L} = \frac{E}{1+\nu}\int_{\mathcal{S}} (\epsilon_{xz}^2 + \epsilon_{yz}^2)\mathrm{d}x\mathrm{d}y = \frac{E\tau^2}{1+\nu}\int_{\mathcal{S}} (\bar{\epsilon}_{xz}^2 + \bar{\epsilon}_{yz}^2)\mathrm{d}x\mathrm{d}y = \frac{J\tau^2}{2}, \tag{3.19}$$

where J is the torsion constant.

For a circular cross-section with radius r, $\boldsymbol{n} \parallel \boldsymbol{r}$ so that $Z = 0$ and

$$J = \frac{E}{2(1+\nu)}\int_{\mathcal{S}} (x^2 + y^2)\mathrm{d}x\mathrm{d}y = \frac{\pi E r^4}{4(1+\nu)}. \tag{3.20}$$

As for the bending, we can compute the moment along $\hat{\boldsymbol{e}}_z$ transmitted through a cross-section:

$$M = \int_{\mathcal{S}} [x\sigma_{yz} - y\sigma_{xz}]\mathrm{d}x\mathrm{d}y \tag{3.21}$$

$$= \frac{E\tau}{1+\nu} \int_{\mathcal{S}} [x\bar{\epsilon}_{yz} - y\bar{\epsilon}_{xz}]\mathrm{d}x\mathrm{d}y \tag{3.22}$$

$$= J\tau - \frac{E\tau}{1+\nu} \int_{\mathcal{S}} (\bar{\epsilon}_{xz}\partial_x\bar{Z} + \bar{\epsilon}_{yz}\partial_y\bar{Z})\mathrm{d}x\mathrm{d}y \tag{3.23}$$

$$= J\tau. \tag{3.24}$$

We have used Eqs. (3.15, 3.16), integrated by parts and used the equations of equilibrium.

3.3 Energy and equilibrium equations

The energy of a deformed rod can thus be written

$$U = \frac{1}{2} \int \left[B_1 \kappa^{(1)}(s)^2 + B_2 \kappa^{(2)}(s)^2 + J\tau(s)^2 \right] \mathrm{d}s, \tag{3.25}$$

where the bending moduli B_1 and B_2 have been computed in Sec. 2.2 and the twist modulus J has been computed in Sec. 3.2.

The moment exerted through a cross-section of the rod is

$$\boxed{\boldsymbol{M}(s) = B_1 \kappa^{(1)}(s)\boldsymbol{d}_1(s) + B_2 \kappa^{(2)}(s)\boldsymbol{d}_2(s) + J\tau(s)\boldsymbol{d}_3(s).} \tag{3.26}$$

Now consider a rod submitted to a linear density of forces $\boldsymbol{f}(s)$ and moments $\boldsymbol{q}(s)$, as before, the balance of forces and moments on the portion $[s, s+\delta s]$ of the rod give

$$\boxed{\begin{aligned} \boldsymbol{F}'(s) + \boldsymbol{f}(s) &= 0, \\ \boldsymbol{M}'(s) + \boldsymbol{d}_3(s) \times \boldsymbol{F}(s) + \boldsymbol{q}(s) &= 0. \end{aligned}} \tag{3.27, 3.28}$$

These equations can be obtained from the variation of the energy (3.25), but the calculation is cumbersome due to the way $\kappa^{(1)}$, $\kappa^{(2)}$ and τ depend on the configuration of the rod [Audoly and Pomeau, 2010, Sec. 3.6].

3.4 Invariants

We will derive invariants for an isotropic ($B_1 = B_2 = B$) rod with $\boldsymbol{f}(s) = 0$ and $\boldsymbol{q}(s) = 0$. As a consequence, $\boldsymbol{F}$ is a constant and the equation for the moment is

$$\boldsymbol{M}'(s) + \boldsymbol{d}_3(s) \times \boldsymbol{F} = 0. \tag{3.29}$$

Taking the scalar product with $\boldsymbol{F}$, we get

$$0 = \boldsymbol{M}'(s) \cdot \boldsymbol{F} + [\boldsymbol{d}_3(s) \times \boldsymbol{F}] \cdot \boldsymbol{F} = \frac{\mathrm{d}}{\mathrm{d}s}[\boldsymbol{M}(s) \cdot \boldsymbol{F}] : \tag{3.30}$$

this is the first invariant:

$$\boxed{\frac{\mathrm{d}}{\mathrm{d}s}[\boldsymbol{F} \cdot \boldsymbol{M}(s)] = 0.} \tag{3.31}$$

Taking the scalar product with $\boldsymbol{d}_3(s)$, we get

$$0 = \boldsymbol{M}'(s) \cdot \boldsymbol{d}_3(s) = \frac{\mathrm{d}}{\mathrm{d}s}[\boldsymbol{M}(s) \cdot \boldsymbol{d}_3(s)] - \boldsymbol{M}(s) \cdot \boldsymbol{d}_3'(s). \tag{3.32}$$

On one hand, from Eq. (3.26),

$$\boldsymbol{M}(s) = B[\kappa^{(1)}(s)\boldsymbol{d}_1(s) + \kappa^{(2)}(s)\boldsymbol{d}_2(s)] + J\tau(s)\boldsymbol{d}_3(s) = B\boldsymbol{\Omega}(s) + \alpha(s)\boldsymbol{d}_3(s); \tag{3.33}$$

on the other hand, $\boldsymbol{d}_3'(s) = \boldsymbol{\Omega}(s) \times \boldsymbol{d}_3(s)$, hence

$$\boldsymbol{M}(s) \cdot \boldsymbol{d}_3'(s) = [B\boldsymbol{\Omega}(s) + \alpha(s)\boldsymbol{d}_3(s)] \cdot [\boldsymbol{\Omega}(s) \times \boldsymbol{d}_3(s)] = 0. \tag{3.34}$$

We thus have a second invariant

$$\boxed{\frac{\mathrm{d}}{\mathrm{d}s}[\boldsymbol{d}_3(s) \cdot \boldsymbol{M}(s)] = 0.} \tag{3.35}$$

The last invariant is obtained by taking the scalar product with $\boldsymbol{\Omega}(s)$:

$$0 = \boldsymbol{M}'(s) \cdot \boldsymbol{\Omega}(s) + [\boldsymbol{d}_3(s) \times \boldsymbol{F}] \cdot \boldsymbol{\Omega}(s). \tag{3.36}$$

From the expression of the moment with the curvatures and $\boldsymbol{d}_i' = \boldsymbol{\Omega} \times \boldsymbol{d}_i$, we see that

$$\boldsymbol{M}'(s) \cdot \boldsymbol{\Omega}(s) = B\left[\kappa^{(1)\prime}(s)\kappa^{(1)}(s) + \kappa^{(2)\prime}(s)\kappa^{(2)}(s)\right] + J\tau'(s)\tau(s) = \frac{1}{2}\frac{\mathrm{d}}{\mathrm{d}s}[\boldsymbol{M}(s) \cdot \boldsymbol{\Omega}(s)]. \tag{3.37}$$

We have for the other term

$$[\boldsymbol{d}_3(s) \times \boldsymbol{F}] \cdot \boldsymbol{\Omega}(s) = [\boldsymbol{\Omega}(s) \times \boldsymbol{d}_3(s)] \cdot \boldsymbol{F} = \boldsymbol{d}_3'(s) \cdot \boldsymbol{F} = \frac{\mathrm{d}}{\mathrm{d}s}[\boldsymbol{d}_3(s) \cdot \boldsymbol{F}]. \tag{3.38}$$

This gives the invariant

$$\boxed{\frac{\mathrm{d}}{\mathrm{d}s}\left[\frac{1}{2}\boldsymbol{\Omega}(s) \cdot \boldsymbol{M}(s) + \boldsymbol{F} \cdot \boldsymbol{d}_3(s)\right] = 0.} \tag{3.39}$$

3.5 Localized helix

We consider an infinite isotropic rod (initially along $\boldsymbol{e}_z$) submitted to a tension T ($\boldsymbol{F} = T\boldsymbol{e}_z$) and a moment M ($\boldsymbol{M}(\pm\infty) = M\boldsymbol{e}_z$). We denote $\boldsymbol{d}_3(s) = \boldsymbol{t}(s)$ and assume that the rod is straight at infinity ($\boldsymbol{t}(\pm\infty) = \boldsymbol{e}_z$). We compute the shape of this rod.

We start by computing the three invariants:

$$\boldsymbol{F} \cdot \boldsymbol{M} = T\boldsymbol{e}_z \cdot \boldsymbol{M} = TM, \tag{3.40}$$

$$\boldsymbol{t} \cdot \boldsymbol{M} = M, \tag{3.41}$$

$$\frac{1}{2}\boldsymbol{\Omega} \cdot \boldsymbol{M} + \boldsymbol{F} \cdot \boldsymbol{t} = \frac{M^2}{2J} + T, \tag{3.42}$$

since at infinity the deformation of the rod is pure twist.

Then we describe the shape of the rod. We use spherical coordinates to represent the tangent vector $\boldsymbol{t}(s)$:

$$\boldsymbol{t}(s) = \sin(\theta(s))\boldsymbol{e}_r(\psi(s)) + \cos(\theta(s))\boldsymbol{e}_z. \tag{3.43}$$

The derivative is

$$\boldsymbol{t}' = \psi' \sin(\theta)\boldsymbol{e}_\psi + \theta'[\cos(\theta)\boldsymbol{e}_r(\psi) - \sin(\theta)\boldsymbol{e}_z]. \tag{3.44}$$

We have to write the vectors $\boldsymbol{\Omega}(s)$ and $\boldsymbol{M}(s)$ as a function of $\theta(s)$ and $\psi(s)$. First, since $\boldsymbol{t}'(s) = \boldsymbol{\Omega} \times \boldsymbol{t}$ and $\boldsymbol{\Omega} \cdot \boldsymbol{t} = \tau$, we see by a quick calculation in the base $(\boldsymbol{d}_1, \boldsymbol{d}_2, \boldsymbol{t})$ that

$$\boldsymbol{\Omega} = \boldsymbol{t} \times \boldsymbol{t}' + \tau \boldsymbol{t}. \tag{3.45}$$

The moment is thus

$$\boldsymbol{M} = B\boldsymbol{t} \times \boldsymbol{t}' + J\tau \boldsymbol{t}. \tag{3.46}$$

In the base $(\boldsymbol{e}_r, \boldsymbol{e}_\psi, \boldsymbol{e}_z)$, the vector product reads

$$\boldsymbol{t} \times \boldsymbol{t}' = \begin{pmatrix} \sin(\theta) \\ 0 \\ \cos(\theta) \end{pmatrix} \times \begin{pmatrix} \theta' \cos(\theta) \\ \psi' \sin(\theta) \\ -\theta' \sin(\theta) \end{pmatrix} = \begin{pmatrix} -\psi' \sin(\theta)\cos(\theta) \\ \theta' \\ \psi' \sin(\theta)^2 \end{pmatrix}. \tag{3.47}$$

Let's now use the invariants. The simplest to use is $\boldsymbol{t} \cdot \boldsymbol{M} = M$, leading to

$$J\tau(s) = M. \tag{3.48}$$

$\boldsymbol{e}_z \cdot \boldsymbol{M} = M$ leads to $B\psi' \sin(\theta)^2 + J\tau\cos(\theta) = M$, and with the previous result,

$$\psi' = \frac{M}{B} \frac{1 - \cos(\theta)}{\sin(\theta)^2}. \tag{3.49}$$

For the last one, $\boldsymbol{\Omega} \cdot \boldsymbol{M} = B|\boldsymbol{t} \times \boldsymbol{t}'|^2 + J\tau^2$; using $|\boldsymbol{t} \times \boldsymbol{t}'|^2 = \boldsymbol{t}'^2 = \theta'^2 + \psi'^2 \sin(\theta)^2$ and $J\tau = M$, we get

$$\frac{B}{2}\left[\theta'^2 + \psi'^2 \sin(\theta)^2\right] = T[1 - \cos(\theta)]. \tag{3.50}$$

Combining this relation with the expression of ψ', we get

$$\boxed{\frac{\theta'^2}{2} + \frac{T}{B} V_\gamma(\theta) = 0,} \tag{3.51}$$

where

$$\boxed{\gamma = \frac{M^2}{4BT}} \tag{3.52}$$

and

$$\boxed{V_\gamma(\theta) = 2\gamma \left[\frac{1 - \cos(\theta)}{\sin(\theta)}\right]^2 - 1 + \cos(\theta).} \tag{3.53}$$

This describes the trajectory of an inertial particle with 0 energy in the potential $V_\gamma(\theta)$, with the condition $\theta(\pm\infty) = 0$.

The expansion of the potential (Fig. 3.1) around 0 is

$$V_\gamma(\theta) = \frac{\gamma - 1}{2}\theta^2 + \mathcal{O}(\theta^4). \tag{3.54}$$

If $\gamma > \gamma_c = 1$, the position $\theta = 0$ is a stable minimum: the rod remains straight. If $\gamma < \gamma_c$ the position $\theta = 0$ is unstable: the rod buckles.

For $\gamma < \gamma_c$ we can obtain an analytical solution. Changing variable for $u = \cos(\theta)$, we have

$$\frac{u'^2}{2} + \frac{T}{B}(1 - u)^2(2\gamma - 1 - u) = 0. \tag{3.55}$$

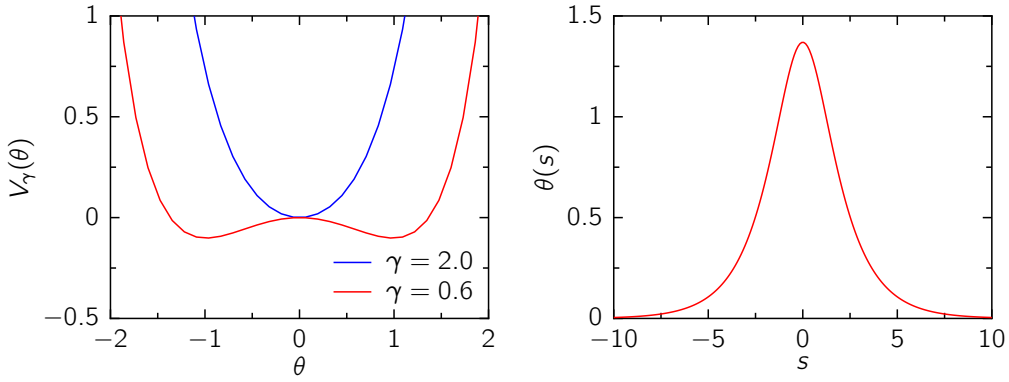

Figure 3.1: *Left:* potential $V_\gamma(\theta)$ of the localized helix for two values of γ. *Right:* solution $\theta(s)$ for $\gamma = 0.6$.

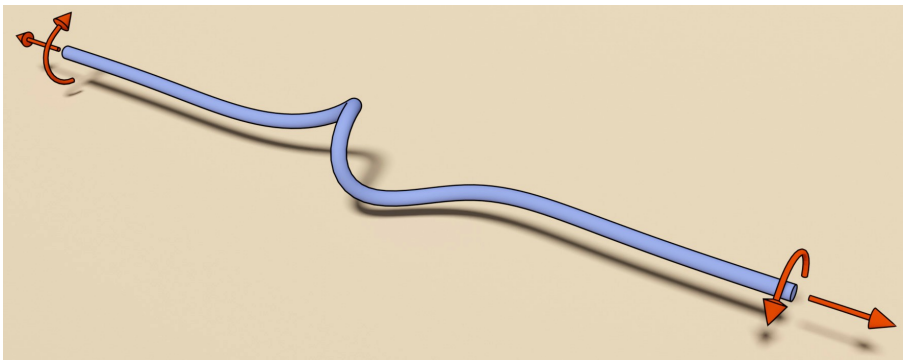

Figure 3.2: Rendering of the localized helix for $\gamma = 0.6$.

Further changing to v such that $2\gamma - 1 - u = -2(1-\gamma)v$, the equation is

$$\frac{v'^2}{2} = \frac{2(1-\gamma)T}{B} v(1-v)^2. \tag{3.56}$$

Noticing that $\tanh' = 1 - \tanh^2$, so that $[(\tanh^2)']^2 = 4\tanh^2(1-\tanh^2)^2$, the solution is

$$v(s) = \tanh\left(\sqrt{\frac{(1-\gamma)T}{B}}(s - s_0)\right)^2, \tag{3.57}$$

where s_0 is the "center" of the helix (the problem is invariant by translation along s). For $\theta(s)$ and $u(s)$, the solution reads

$$\boxed{u(s) = \cos(\theta(s)) = 2\gamma - 1 + 2(1-\gamma)\tanh\left(\sqrt{\frac{(1-\gamma)T}{B}}(s - s_0)\right)^2.} \tag{3.58}$$

We note that $\theta(s) \to 0$ as $s \to \pm\infty$, as expected. A solution for $\gamma = 0.6$ is shown on Fig. 3.2.

This localized pattern is reminiscent of the wrinkle localization into a fold discussed in Sec. 2.6.2.

Chapter 4

Sheets

4.1 Geometry and mechanics of sheets

4.1.1 Stretching and bending moduli

Consider a sheet submitted to a strain ϵ_{xx} in the x direction, with a vanishing stress in the y direction, $\sigma_{yy} = 0$. With the Hooke's law for plane stress, Eq. (2.2) (here $\sigma_{zz} = 0$), from $\sigma_{yy} = 0$ we get $\epsilon_{yy} = -\nu\epsilon_{xx}$, hence

$$\sigma_{xx} = \frac{E}{1+\nu}\left[\epsilon_{xx} + \frac{\nu}{1-\nu}(\epsilon_{xx} + \epsilon_{yy})\right] = E\epsilon_{xx}. \tag{4.1}$$

The energy density integrated over the thickness is thus

$$e = \frac{t}{2}\sigma_{xx}\epsilon_{xx} = \frac{Et}{2}\epsilon_{xx}^2, \tag{4.2}$$

which defines the stretching modulus

$$\boxed{Y = Et.} \tag{4.3}$$

The case of bending has been adressed in Sec. 2.5: imposing a curvature $\kappa_x = 1/R_x$ in the x direction leads to an energy per unit area

$$e = \frac{B}{2}\kappa_x^2, \tag{4.4}$$

where the bending modulus is (Eq. (2.32)):

$$\boxed{B = \frac{Et^3}{12(1-\nu^2)}.} \tag{4.5}$$

4.1.2 Gauss theorema egregium

4.1.2.1 Theorem

We consider a sheet with rest configuration

$$\boldsymbol{R}^0(x,y) = \begin{pmatrix} x \\ y \\ 0 \end{pmatrix}. \tag{4.6}$$

The reference metric $g^0_{ij} = \partial_i \boldsymbol{R}^0 \cdot \partial_j \boldsymbol{R}^0$ is simply

$$g^0 = \begin{pmatrix} 1 & 0 \\ 0 & 1 \end{pmatrix}. \tag{4.7}$$

We consider a deformation of the sheet into

$$\boldsymbol{R}(x,y) = \begin{pmatrix} x + u(x,y) \\ y + v(x,y) \\ w(x,y) \end{pmatrix}. \tag{4.8}$$

The metric is now

$$g = \begin{pmatrix} (1+u_x)^2 + v_x^2 + w_x^2 & (1+u_x)u_y + v_x(1+v_y) + w_x w_y \\ (1+u_x)u_y + v_x(1+v_y) + w_x w_y & u_y^2 + (1+v_y)^2 + w_y^2 \end{pmatrix}, \tag{4.9}$$

where we denote the partial derivatives with indices: $\partial_x u = u_x$, etc.

We consider small deformations, and we want to expand to the lowest non trivial order in the displacements u, v and w. We see in the term g_{xx} that the term u_x compares to w_x^2, thus we retain terms of order two in w and one in u. This gives for the strain

$$\boxed{\epsilon = \frac{g - g^0}{2} = \begin{pmatrix} u_x + \frac{w_x^2}{2} & \frac{u_y + v_x + w_x w_y}{2} \\ \frac{u_y + v_x + w_x w_y}{2} & v_y + \frac{w_y^2}{2} \end{pmatrix}.} \tag{4.10}$$

We are interested in the curvature of the sheet, which is encoded in the out of plane displacement w. To get rid of the in plane displacement, we consider $2\partial_x\partial_y\epsilon_{xy} - \partial_y^2\epsilon_{xx} - \partial_x^2\epsilon_{yy}$:

$$\partial_x\partial_y\epsilon_{xy} = \frac{1}{2}\left(u_{xyy} + v_{xxy} + w_{xxy}w_y + w_{xy}^2 + w_{xx}w_{yy} + w_x w_{xyy}\right), \tag{4.11}$$

$$\partial_y^2\epsilon_{xx} = u_{xyy} + w_{xy}^2 + w_x w_{xyy}, \tag{4.12}$$

$$\partial_x^2\epsilon_{yy} = v_{xxy} + w_{xy}^2 + w_y w_{xxy}. \tag{4.13}$$

Hence

$$\boxed{2\partial_x\partial_y\epsilon_{xy} - \partial_y^2\epsilon_{xx} - \partial_x^2\epsilon_{yy} = w_{xx}w_{yy} - w_{xy}^2 = \det(w_{ij}).} \tag{4.14}$$

This is Gauss' theorema egregrium (remarkable theorem).

4.1.2.2 Gauss curvature

The right hand side is the Gauss curvature κ_G. The tensor w_{ij} is symmetric, hence there is an orthogonormal base where it is diagonal; choosing this base, w reads

$$w(x,y) = \frac{x^2}{2R_x} + \frac{y^2}{2R_y}, \tag{4.15}$$

where R_x and R_y are the two principal radii of curvature ($\kappa_i = 1/R_i$ is the corresponding curvature). Then

$$w_{\alpha\beta} = \begin{pmatrix} R_x^{-1} & 0 \\ 0 & R_y^{-1} \end{pmatrix} \tag{4.16}$$

and

$$\kappa_G = \det(w_{ij}) = \frac{1}{R_x R_y}. \tag{4.17}$$

The main implication of this theorem is that if the Gauss curvature is non-zero (the sheet is bent in two directions), the strain cannot vanish. Since bending is energetically cheap and stretching is expansive, this is some kind of geometric frustration: bending in direction x is cheap, bending in direction y is also cheap, but bending in the two directions is expensive.

4.1.2.3 Application to the sheet-on-sphere adhesion

By dimensional arguments, the "geometrical strain" required to apply a Gauss curvature κ_G to a sheet of lateral size L is thus

$$\epsilon_{\text{Gauss}} \sim \kappa_G L^2. \tag{4.18}$$

The stretching energy of a flat disc of radius L on a sphere of radius $R \gg L$ [Majidi and Fearing, 2008], where $\kappa_G = R^{-2}$ is

$$U_{\text{stretch}} \sim Y L^2 \epsilon_{\text{Gauss}}^2 \sim Y \kappa_G^2 L^6 \sim \frac{Y L^6}{R^4}. \tag{4.19}$$

The bending energy in this situation is

$$U_{\text{bend}} \sim \frac{B L^2}{R^2} \sim \frac{Y t^2 L^2}{R^2}. \tag{4.20}$$

With an adhesion energy Γ per unit area, if the sheet is sufficiently thin ($R > \ell_{\text{BC}} = \sqrt{B/\gamma}$), the stretching energy sets the threshold for delamination, which is thus [Hure et al., 2011]

$$\Gamma L^2 \sim \frac{Y L^6}{R^4}. \tag{4.21}$$

4.1.2.4 3d shape design by prescribing the metric

Gauss's theorem gives a relation between the strain and the out-of-plane deformation. The strain being given as the difference between the actual and the target metric, this is actually a relation between the out-of-plane displacement and the metric. Prescribing a non-flat metric g^0, out-of-plane displacement may be needed have a vanishing strain.

Prescribing a non-flat metric can be done by using gels that have a non-uniform response to a solvent [Klein et al., 2007, Sharon and Efrati, 2010] or a temperature change [Kim et al., 2012].

Note that the mapping between the metric and the out-of-plane displacement is not straightforward: a torn plastic sheet has a metric of the form [Marder et al., 2003]

$$g^0 = \begin{pmatrix} 1 + \alpha \mathrm{e}^{-y/\xi} & 0 \\ 0 & 1 \end{pmatrix}, \tag{4.22}$$

where $x \in \mathbb{R}$ and $y \geq 0$. The line $y = 0$ being compressed in the flat state ($\epsilon_{xx} = \frac{1}{2}(g_{xx} - g^0_{xx}) = -\alpha/2$), it buckles. Surprisingly, the buckling pattern is fractal [Sharon et al., 2002].

Finally, incompatibility between the target metric and the "spontaneous curvature" of the material can lead to specific buckling patterns, which occur for instance in plants [Armon et al., 2011].

4.1.3 Föppl-von Kármán equations

The in-plane strain ϵ_{ij} is given as a function of the displacements u, v and w (in and out of plane) in Eq. (4.10), and the in-plane stress σ_{ij} can be deduced using the Hooke's law in 2d using plane stress conditions, Eq. (2.2). For plates, it is easier to use the planar stress instead of the volumic stress, hence the stretching modulus $Y = Et$ has to be used instead of the Youngs modulus in Hooke's law:

$$\sigma_{ij} = \frac{Y}{1+\nu}\left(\epsilon_{ij} + \frac{\nu}{1-\nu}\epsilon^{(2)}_{kk}\delta_{ij}\right). \tag{4.23}$$

The in-plane force balance is analogous to the 3d force balance:

$$\partial_i \sigma_{ij} = 0. \tag{4.24}$$

For the out-of-plane force balance, a direct derivation is cumbersome [Audoly and Pomeau, 2010, Secs. 6.4 and 6.5] so we resort to the equilibrium equation of a rod derived in Sec. 2.3, that we generalize to a plate. We consider a rod that is nearly straight, so that we can replace s by x, and the height $w(x)$ is related to the angle $\theta(x)$ through $\theta(x) = w'(x)$. The moment exerted through the rod is thus $M(x) = B\theta'(x) = Bw''(x)$, where the bending moment is the bending moment of a plate, Eq. (2.32). The tangent vector is

$$\boldsymbol{t}(x) = \begin{pmatrix} 1 \\ w'(x) \end{pmatrix}, \tag{4.25}$$

and the force is given by the in-plane tension:

$$\boldsymbol{F}(x) = \begin{pmatrix} \sigma_{xx}(x) \\ 0 \end{pmatrix}. \tag{4.26}$$

The equation for the equilibrium of momentum is thus

$$Bw'''(x) - w'(x)\sigma_{xx}(x) = 0. \tag{4.27}$$

Deriving, we arrive at

$$B\partial_x^4 w = \partial_x(\sigma_{xx}\partial_x w). \tag{4.28}$$

The two-dimensional generalization is

$$B\nabla^4 w = \partial_i(\sigma_{ij}\partial_j w), \tag{4.29}$$

where $\nabla^4 = (\partial_x^2 + \partial_y^2)^2$. The derivative on the right hand side can be developped, and using the in-plane force balance we get $\partial_i(\sigma_{ij}\partial_j w) = \sigma_{ij}\partial_i\partial_j w$.

Finally, we obtain the Föppl-von Kármán equations:

$$\boxed{\begin{aligned} \partial_i\sigma_{ij} &= 0, && (4.30)\\ B\nabla^4 w - \sigma_{ij}\partial_i\partial_j w &= 0. && (4.31) \end{aligned}}$$

External forces can be added in these equations. For instance, if a pressure P is applied below the plate the out-of-plane equation becomes

$$B\nabla^4 w - \sigma_{ij}\partial_i\partial_j w = P. \tag{4.32}$$

Note that without the bending modulus, this equation is a generalization of the Laplace law, $-\gamma\nabla^2 w = P$.

The Föppl-von Kármán equations can be derived from the elastic energy that contains stretching and bending contributions. However, the exact form of the energy is not straightforward [Audoly and Pomeau, 2010, Sec. 6.6], and in general the scaling of the two contributions is enough to get the required scalings.

We have given here the Föppl-von Kármán equations for small deviations to a flat configuration. However, when there are large deviations to a flat configuration, one has to use a covariant expression of these equations [Dias et al., 2011]. For instance, the derivatives present in the Föppl-von Kármán equations have to be replaced by covariant derivatives, based on the metric of the sheet. This formalism has proven useful to compute the stress in a stretched and twisted ribbon [Chopin et al., 2015].

4.1.4 Reduced models

The Föppl-von Kármán equations are non-linear and may thus be difficult to solve. For this reason it is always useful to have reduced models to address situations where some effects are irrelevant.

4.1.4.1 Membrane model

Neglecting the bending contribution in Eq. (4.31), we obtain the membrane model. However, we know from the study of buckling (Sec. 2.4 and Sec. 2.6) that without bending modulus there is no resistance to compression, meaning that any level of compression is relaxed by tiny wrinkles, which cannot be described by the membrane model. The absence of compressive stress should be added to the equations:

$$\sigma_{ii} \geq 0, \tag{4.33}$$

for any direction i.

4.1.4.2 Geometric model

An even further simplification if the loading is too weak to stretch the sheet is to consider the sheet as inextensible. This can be called a "geometric" model, in the sense that there is no elastic modulus anymore.

For example, a geometric model has been used to understand the shape of a Mylar balloon [Paulsen, 1994]; we quickly review its approach here. A Mylar balloon is made of two flat discs glued together at the edges, and then inflated. Assuming that Mylar is inextensible, once under pressure, the balloon takes the shape that maximizes its volume under the constraint of inextensibility.

Taking a cut of the balloon along its symmetry axis, a quarter of the shape can be described by a function $y(x) \geq 0$ for $0 \leq x \leq a$, where a is the radius of the inflated balloon, such that $y(a) = 0$. The volume V of the balloon and half length of a meridian R (the radius of the disks) are given by

$$V = 4\pi \int_0^a xy(x)\mathrm{d}x, \tag{4.34}$$

$$R = \int_0^a \sqrt{1 + y'(x)^2}\mathrm{d}x \tag{4.35}$$

The functionnal to minimize is thus

$$I[y] = \int_0^a \left[xy(x) - \lambda\sqrt{1 + y'(x)^2}\right] \mathrm{d}x, \tag{4.36}$$

where λ is a Lagrange multiplier and we have factored out 4π.

The corresponding Euler-Lagrange equation reads

$$-\lambda \frac{\mathrm{d}}{\mathrm{d}x}\left[\frac{y'(x)}{\sqrt{1 + y'(x)^2}}\right] = x. \tag{4.37}$$

It can be shown rigorously that the boundary conditions are $y'(0) = 0$, $y'(a) = -\infty$. Integrating the above equation between 0 and x leads to

$$\frac{y'(x)}{\sqrt{1 + y'(x)^2}} = -\frac{x^2}{a^2}, \tag{4.38}$$

Where we have used $y'(a) = -\infty$ to show that $\lambda = a^2/2$. This relation can be inverted, leading to

$$y'(x) = -\frac{x^2}{\sqrt{a^4 - x^4}}. \tag{4.39}$$

This completely defines the solution through an elliptic integral:

$$y(x) = \int_x^a \frac{x'^2}{\sqrt{a^4 - x'^4}} \mathrm{d}x'. \tag{4.40}$$

This approach is purely geometric and bypasses the complex pattern of the wrinkles and "crumples" that appear in these balloons. The calculation could also be done using mechanical arguments, such as the ones Taylor used to compute the optimal shape of a parachute [Taylor, 1919]. Quite surprisingly, the parachute has the same shape as the balloon.

4.1.5 Numerical simulations

A minimal numerical model for elastic sheets has been introduced by Seung and Nelson [1988]. In this model, the sheet consists in a triangular lattice of "beads" attached by springs; this generates a stretching modulus. A bending modulus is obtained with an energy penalty for the angle between neighboring facets. We first introduce this model and then compute the elastic moduli of the corresponding sheet.

Denoting $\boldsymbol{R}_a$ the position of the bead a, the stretching energy is given by

$$U_{\mathrm{str}} = \frac{k}{2} \sum_{\langle a,b \rangle} \left(|\boldsymbol{R}_a - \boldsymbol{R}_b| - \ell \right)^2, \tag{4.41}$$

where k is the spring constant, ℓ is the rest length of the springs, and $\langle a, b \rangle$ are nearest neighbours. Denoting $\hat{\boldsymbol{n}}_\alpha$ the unit normal to the facet α, the bending energy is

$$U_{\mathrm{bend}} = \kappa \sum_{\langle \alpha,\beta \rangle} (1 - \hat{\boldsymbol{n}}_\alpha \cdot \hat{\boldsymbol{n}}_\beta). \tag{4.42}$$

We can compute the effective properties of this sheet. If $\boldsymbol{r}_a$ denotes the initial position of the bead a, then

$$(\boldsymbol{R}_a - \boldsymbol{R}_b)^2 \simeq g_{ij} (\boldsymbol{r}_a^i - \boldsymbol{r}_b^i)(\boldsymbol{r}_a^j - \boldsymbol{r}_b^j) = \ell^2 \left[1 + 2\epsilon_{ij} d^i \hat{d}^j \right], \tag{4.43}$$

where $\boldsymbol{r}_a - \boldsymbol{r}_b = \ell \hat{\boldsymbol{d}}$. Finally,

$$|\boldsymbol{R}_a - \boldsymbol{R}_b| - \ell \simeq \ell \epsilon_{ij} d^i \hat{d}^j. \tag{4.44}$$

We can now sum the square over the three sides of a facet, where $\hat{\boldsymbol{d}} = (1, 0)$, $\left(\frac{1}{2}, \frac{\sqrt{3}}{2}\right)$ or $\left(\frac{1}{2}, -\frac{\sqrt{3}}{2}\right)$; after a few lines we get

$$\sum_{\mu=1}^{3} \left(\epsilon_{ij} d_\mu^i \hat{d}_\mu^j \right)^2 = \frac{3}{4} \epsilon_{ij} \epsilon_{ij} + \frac{3}{8} (\epsilon_{kk})^2. \tag{4.45}$$

With the area of a facet, $\sqrt{3}\ell^2/4$, and taking into account the fact that the bonds are shared between two facets, we get an energy density

$$U_{\mathrm{str}} = \frac{\sqrt{3}k}{4} \left[\epsilon_{ij} \epsilon_{ij} + \frac{1}{2} (\epsilon_{kk})^2 \right]. \tag{4.46}$$

This should be compared to the continuous energy density

$$U_{\mathrm{str}} = \frac{1}{2} \epsilon_{ij} \sigma_{ij} = \frac{Y}{2(1+\nu)} \left[\epsilon_{ij} \epsilon_{ij} + \frac{\nu}{1-\nu} (\epsilon_{kk})^2 \right]. \tag{4.47}$$

We get

$$Y = \frac{2}{\sqrt{3}}k, \tag{4.48}$$

$$\nu = \frac{1}{3}. \tag{4.49}$$

We note that the Poisson ratio is set by the geometry of the lattice. This could have been expected because there was no dimensionless parameter in the model.

For the bending energy we use a simple derivation, where the sheet is bent in a single direction, so that only the bonds "$(1,0)$" are bent by an angle $\theta \ll 1$. The distance between two lines of bending is $\ell' = \sqrt{3}\ell/2$, and the curvature is $c = \theta/\ell'$. The energy of a single bond is $\kappa(1 - \hat{\boldsymbol{n}}_\alpha \cdot \hat{\boldsymbol{n}}_\beta) \simeq \kappa\theta^2/2$. The density of these bonds is $(\ell\ell')^{-1}$, hence the energy density is

$$U_{\text{bend}} = \frac{\kappa\theta^2}{2\ell\ell'} = \frac{\sqrt{3}}{4}\kappa c^2 = \frac{Bc^2}{2}, \tag{4.50}$$

leading to the bending modulus

$$B = \frac{\sqrt{3}}{2}\kappa. \tag{4.51}$$

Note that without the prefactors, the relations could have been obtained by simple dimensionnal analysis: $Y \sim k$, $B \sim \kappa$. The effective thickness is given by $t \sim \sqrt{B/Y} \sim \sqrt{\kappa/k}$.

4.2 Instabilities, pattern formation

4.2.1 Wrinkles

Wrinkles are a special kind of buckling pattern forming in a variety of situations such as a poked inflated balloon [Vella et al., 2011], a hand streched band [Cerda and Mahadevan, 2003], or a drop supporting sheet on a liquid interface [Huang et al., 2007]. The main questions regarding wrinkles are: When do they form? What are their wavelength and amplitude?

As in the one dimensional case, there are two main approaches: considering the system close to the instability threshold or far from the threshold, deep in the buckled state. Close to the threshold, we typically perform a linear stability analysis, leading to the threshold and the wavelength. The stability analysis is performed around a well-known state, and assumes that the wrinkles are a small perturbation to this state (displacement and stress fields). Far from the threshold, there is no reference state to expand around, so additional inputs are needed.

First we see how these approaches organize on a simple problem, and then we discuss qualitatively other phenomena.

4.2.1.1 Lamé problem

Setup. The "Lamé setup" is shown Fig. 4.1. The idea is to apply different tensions on the inner and outer edges (T_{in} and T_{out}) of an annular sheet. To do so, the sheet is placed at a water-air interface and a surfactant is added outside of the annulus, the tension is thus lower on the outer edge ($T_{\text{out}} < T_{\text{in}}$). Moving a barrier allows to compress the surfactant layer and thus to lower the outer surface tension. This setup has been developed by Piñeirua et al. [2013] and used with thinner sheets by Paulsen et al. [2017]. Géminard et al. [2004] have used a setup with the same geometry but applying loads differently.

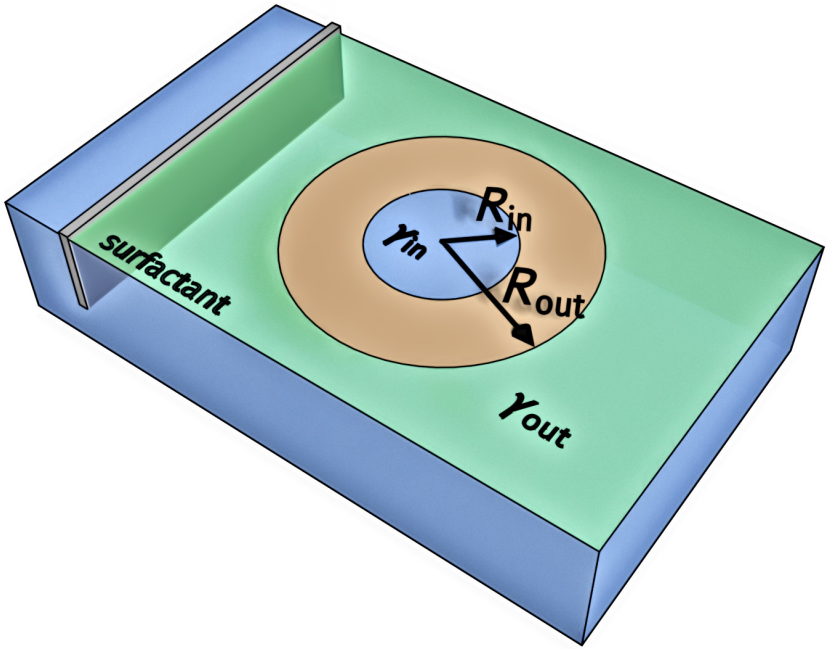

Figure 4.1: Lamé setup

The main parameters are the inner and outer radii R_{in} and R_{out}, and the inner and outer surface tension T_{in} and T_{out}. In experiments, T_{out} is lowered. At some point, wrinkles form near the inner edge and expand.

Flat state. We start by computing the displacement and stress field in the flat state. Due to the axial symmetry of the problem, the displacement is radial and depends on the distance r to the center of the annulus, we denote it $u(r)$. The displacement is the function that we have to determine. The strain in the radial and azimuthal directions can easily be computed:

$$\epsilon_{rr}(r) = \partial_r u(r), \tag{4.52}$$

$$\epsilon_{\theta\theta}(r) = \frac{u(r)}{r}. \tag{4.53}$$

It is related to the stress through Hooke's law (2.2).

The force balance equation can be determined either by considering the forces on a small piece of sheet or by using covariant elasticity with the metric corresponding to the polar coordinates. Due to the symmetry of the problem, it provides an equation only in the direction r:

$$\partial_r[r\sigma_{rr}(r)] = \sigma_{\theta\theta}. \tag{4.54}$$

Finally, the boundary conditions are:

$$\sigma_{rr}(R_{\text{in}}) = T_{\text{in}}, \tag{4.55}$$

$$\sigma_{rr}(R_{\text{out}}) = T_{\text{out}}. \tag{4.56}$$

The Hooke's law gives

$$\frac{\sigma_{rr}(r)}{E} = \frac{u'(r)}{1-\nu} + \frac{\nu}{1-\nu^2}\frac{u(r)}{r}, \tag{4.57}$$

$$\frac{\sigma_{\theta\theta}(r)}{E} = \frac{1}{1-\nu}\frac{u(r)}{r} + \frac{\nu}{1-\nu^2}u'(r). \tag{4.58}$$

The radial force balance (4.54) thus becomes

$$\partial_r\left[ru'(r)\right] = \frac{u(r)}{r}. \tag{4.59}$$

Looking for a solution of the form $u(r) = r^\alpha$, we get $\alpha^2 = 1$, hence

$$u(r) = Ar + \frac{B}{r}. \tag{4.60}$$

Hence

$$\sigma_{rr}(r) = E\left(\frac{1+2\nu}{1-\nu^2}A - \frac{1}{1-\nu^2}\frac{B}{r^2}\right) = A' + \frac{B'}{r^2}. \tag{4.61}$$

Using the boundary conditions (4.55, 4.56), we obtain

$$\sigma_{rr}(r) = \frac{R_{\rm out}^2 T_{\rm out} - R_{\rm in}^2 T_{\rm in}}{R_{\rm out}^2 - R_{\rm in}^2} + \frac{T_{\rm in} - T_{\rm out}}{R_{\rm in}^{-2} - R_{\rm out}^{-2}}\frac{1}{r^2}, \tag{4.62}$$

$$\sigma_{\theta\theta}(r) = \frac{R_{\rm out}^2 T_{\rm out} - R_{\rm in}^2 T_{\rm in}}{R_{\rm out}^2 - R_{\rm in}^2} - \frac{T_{\rm in} - T_{\rm out}}{R_{\rm in}^{-2} - R_{\rm out}^{-2}}\frac{1}{r^2}. \tag{4.63}$$

where we have used the force balance (4.54) to compute the azimuthal stress. Introducing

$$T_\infty = \frac{R_{\rm out}^2 T_{\rm out} - R_{\rm in}^2 T_{\rm in}}{R_{\rm out}^2 - R_{\rm in}^2} < T_{\rm in}, \tag{4.64}$$

the stress field can be written as

$$\sigma_{rr}(r) = T_\infty + (T_{\rm in} - T_\infty)\frac{R_{\rm in}^2}{r^2}, \tag{4.65}$$

$$\sigma_{\theta\theta}(r) = T_\infty - (T_{\rm in} - T_\infty)\frac{R_{\rm in}^2}{r^2}. \tag{4.66}$$

As $\sigma_{\theta\theta}(R_{\rm in}) = 2T_\infty - T_{\rm in}$, the inner edge is under compression for $T_\infty < T_{\rm in}/2$, and prone to buckling.

Near threshold. We first consider a narrow annulus, $R_{\rm out} \gtrsim R_{\rm in}$, so that the azimuthal stress is almost uniform. Its buckling can be seen as the buckling of a compressed sheet on a liquid, which has been discussed in Sec. 2.6.1. The threshold is thus $\sigma_{\theta\theta} < -2\sqrt{B\rho g}$, and the wavelength should be given by $\lambda = 2\pi(\rho g/B)^{1/4}$; the criterion for the stress can be written

$$\frac{T_\infty}{T_{\rm in}} < \frac{1}{2} - \frac{\ell_{\rm BC}}{\ell_{\rm c}}, \tag{4.67}$$

where $\ell_{\rm c} = \sqrt{T_{\rm in}/(\rho g)}$ is the capillary length. These predictions have been verified experimentally [Piñeirua et al., 2013]. We have neglected the effect of the meniscus of liquid on the inner and outer edges, in the one dimensional analysis of Sec. 2.6.1 the sheet was assumed to be infinite in

the direction perpendicular to the compression. As explained by Piñeirua et al. [2013], this assumption is valid if the annulus is wider than the capillary length and stiff enough to prevent a cascade at its edges, an effect that we discuss below.

The arguments for a narrow annulus provide handwavy arguments for a wider annulus. The threshold for buckling can alternatively obtained by a linear stability analysis, using the out-of-plane Föppl-von Kármán equation (4.32) [Piñeirua et al., 2013]. Denoting $w(r,\theta)$ the vertical displacement of the sheet, the pressure is given by $P=-\rho g w$ and

$$B\nabla^4 w - \sigma_{rr}\left(\partial_r^2 w + \frac{1}{r}\partial_r w\right) - \sigma_{\theta\theta}\frac{1}{r^2}\partial_\theta^2 w + \rho g w = 0. \tag{4.68}$$

Looking for a solution of the form $w(r,\theta)=f(r)\sin(m\theta)$, the above equation becomes a fourth order ODE for $f(r)$. Assuming that the sheet is free of forces and torques at the inner and outer edges leads four boundary conditions. Generically, the only solution to this problem is $f(r)=0$; the linear stability analysis amounts to look for the value of T_{out} where a non-zero solution exists. The value of m leading to the highest value of $T_{\text{out,c}}$ gives the wavelength of the wrinkles, and the form of $f(r)$ gives their extent.

Far from threshold. We assume that we are far above the buckling threshold and want to determine the properties of the wrinkles. In this situation the wrinkles substantially modify the stress field; we take the membrane limit and assume that the wrinkles completely relax the compression: $\sigma_{\theta\theta}=0$ where wrinkles are present, and $\sigma_{\theta\theta}>0$ without wrinkles (the same condition applies to σ_{rr}, but it is always positive) [Davidovitch et al., 2011].

The annulus is thus separated in two regions: a wrinkled region for $R_{\text{in}}<r<W$, where $\sigma_{\theta\theta}=0$ and a flat region for $W<r<R_{\text{out}}$, where $\sigma_{\theta\theta}>0$. In the wrinkled region, the force balance (4.54) gives $\sigma_{rr}(r)=T_{\text{in}}R_{\text{in}}/r$. In the flat region, the equations are the same as above, and the stress field is of the form $\sigma_{rr}(r)=A+B/r^2$, $\sigma_{\theta\theta}(r)=A-B/r^2$. The boundary conditions are $\sigma_{rr}(W)=T_{\text{in}}R_{\text{in}}/W$, $\sigma_{\theta\theta}(W)=0$, and $\sigma_{rr}(R_{\text{out}})=T_{\text{out}}$. The first two equations give $B=AW^2$ and $A=T_{\text{in}}R_{\text{in}}/(2W)$, and the last equation leads to an equation for $x=W/R_{\text{out}}$:

$$x^2+2\alpha x+1=0, \tag{4.69}$$

where

$$\alpha=\frac{T_{\text{out}}R_{\text{out}}}{T_{\text{in}}R_{\text{in}}}. \tag{4.70}$$

This equation has a real solution $x<1$ only if $\alpha>1$, which is

$$x^*=\alpha-\sqrt{\alpha^2-1}. \tag{4.71}$$

Note that there is no solution if $\alpha<1$.

In the wrinkled region, the amplitude and wavelength of the wrinkles are related by a slaving condition anologous to the one seen in Sec. 2.6.1 (Eq. (2.35)). Assuming an out of plane displacement of the form $w(r,\theta)=f(r)\sin(m\theta)$, the relative excess length taken away by the wrinkles at a radius r is $m^2f(r)^2/(4r^2)$ in the limit of small slopes. This strain should be added to the strain of the flat state (Eq. (4.53)):

$$\epsilon_{\theta\theta}(r)=\frac{u(r)}{r}+\frac{m^2f(r)^2}{4r^2}. \tag{4.72}$$

Given the stress field, we can compute the strain through the Hooke's law, which gives $\epsilon_{rr}=\sigma_{rr}/E$ and $\epsilon_{\theta\theta}=-\nu\epsilon_{rr}$ in the wrinkled zone. The strain field can then be integrated to get $u(r)$, so that we finally have determined $mf(r)$ through Eq. (4.72).

We do not discuss further the properties of the wrinkles in this setup, and turn to the different mechanisms that play a role in the selection of the wrinkles wavelength.

4.2.1.2 Selection of the wavelength

In the case of wrinkling at an air-water interface, the wavelength is set by a balance of bending and gravity (Sec. 2.6.1). Bending penalizes short wavelengths, while gravity penalizes large amplitudes, and thus large wavelengths through the slaving condition. In two-dimensionnal settings, other mechanisms may penalize large amplitudes.

If wrinkles have a finite extent L and are submitted to a tension T, the stretching energy along the wrinkles is given by

$$U_{\text{tens}} \sim \epsilon T \sim \left(\frac{A}{L}\right)^2 T. \tag{4.73}$$

This corresponds to an effective stiffness [Cerda and Mahadevan, 2003]

$$K_{\text{tens}} = \frac{T}{L^2}. \tag{4.74}$$

Wrinkles often occur on curved substrates. If the radius of curvature in the direction parallel to the wrinkles is $R_\parallel$, for a profile of the form $f(x) = A\cos(kx)$, the strain along the wrinkles at x is given by $\epsilon_\parallel(x) = f(x)/R_\parallel$. This leads to an average stretching energy

$$U_{\text{str}} \sim Y\left(\frac{A}{R_\parallel}\right)^2, \tag{4.75}$$

corresponding to an effective stiffness

$$K_{\text{curv}} = \frac{Y}{R_\parallel^2}. \tag{4.76}$$

4.2.2 Cascades

When describing the wrinkles that form on a compressed rectangular sheet in Sec. 2.6.1, we have assumed an infinite system in the direction of the wrinkles. However, the compressed sheet is always finite, and the capillary force at the edge of the sheet can modify the wrinkle pattern. As described by Huang et al. [2010], the capillary force favors shorter amplitude and wavelength, leading to a decrease of the wavelength close to the edge, which is a *cascade*.

A cascade is also observed on hanging curtains: the wavelength increases from the top to the bottom. Here we give the general analysis of Vandeparre et al. [2011], which uses the *wrinklon*, the transition zone between the wavelengths λ and 2λ, as the building block of a cascade. Considering that wrinkles with a wavelength λ have an amplitude A such that $\epsilon \sim A^2/\lambda^2$, the bending energy gain per unit area to double the wavelength is

$$U_{\text{bend}} \sim B\left(\frac{A}{\lambda^2}\right)^2 \sim \frac{B\epsilon}{\lambda^2}. \tag{4.77}$$

Here we have neglected the bending energy along the wrinkles. Changing the wavelength over a length L generates a strain $(A/L)^2$, and thus a stretching energy per unit area

$$U_{\text{str}} \sim Y\left(\frac{A}{L}\right)^4 \sim \frac{Y\epsilon^2\lambda^4}{L^4}. \tag{4.78}$$

Balancing these two energies leads to

$$L \sim \epsilon^{1/4} t^{-1/2} \lambda^{3/2}. \tag{4.79}$$

We note that we have set $U_{\text{bend}} \sim U_{\text{str}}$, while in principle we should have minimized $U_{\text{bend}} + U_{\text{str}}$, leading to $L \to \infty$; however, this is the energy per unit area, and minimizing $L\lambda(U_{\text{bend}} + U_{\text{str}})$ gives the result above.

Denoting x the coordinate along the wrinkles, we can obtain an equation for $\lambda(x)$:

$$\frac{\mathrm{d}\lambda}{\mathrm{d}x} \simeq \frac{\lambda}{L} \sim \epsilon^{-1/4} t^{1/2} \lambda^{-1/2}, \tag{4.80}$$

the solution of which is

$$\lambda \sim \epsilon^{-1/6} t^{1/3} x^{2/3}. \tag{4.81}$$

This scaling law has been observed for short curtains [Vandeparre et al., 2011].

If a tension σ is imposed along the wrinkles, this tension dominates over the strain induced by the period doubling if $\sigma \gg Y(A/L)^2$. If this is the case, the dominant stretching energy is

$$U_{\text{str}} \sim \sigma \left(\frac{A}{L}\right)^2 \sim \frac{\sigma \epsilon \lambda^2}{L^2} \tag{4.82}$$

instead of Eq. (4.78). Comparing this energy to the bending energy, we find

$$L \sim \left(\frac{\sigma \lambda^4}{B}\right)^{1/2} \sim \left(\frac{\sigma}{Y}\right)^{1/2} \frac{\lambda^2}{t}. \tag{4.83}$$

With the same argument as above, we have

$$\frac{\mathrm{d}\lambda}{\mathrm{d}x} \sim \left(\frac{\sigma}{Y}\right)^{-1/2} \frac{t}{\lambda}, \tag{4.84}$$

and thus

$$\lambda \sim \left(\frac{\sigma}{Y}\right)^{-1/4} t^{1/2} x^{1/2}. \tag{4.85}$$

This scaling has been observed for long curtains, graphene sheets under tension [Vandeparre et al., 2011], and at the edge of a compressed floating sheet [Huang et al., 2010].

Note that the cascade described here is very different from the cascade observed at the edge of a torn plastic sheet, where the different wavelength superpose [Sharon et al., 2002, Marder et al., 2003, Sharon et al., 2007].

4.2.3 Crumples and folds

When wrinkles are curved, the curvature generate a strain that can play a role in the wavelength selection, as seen in Sec. 4.2.1.2. However, when this curvature is too large the wrinkles are replaced by "crumples"; they can be seen when a flat circular sheet is placed of a drop with increasing curvature [King et al., 2012], or in an inflated Mylar balloon. The precise shape of the crumples, their energy, and the critical curvature where they appear are still unknown.

Sharp folds are another pattern that appear upon compression; they have been observed in a "sheet on drop" experiment [Paulsen et al., 2015] or in the Lamé setup when $T_{\text{in}} R_{\text{in}} > T_{\text{out}} R_{\text{out}}$ (see Sec. 4.2.1.1) [Piñeirua et al., 2013, Paulsen et al., 2017]. For very thin sheets [Paulsen et al., 2015, 2017], the folds have been shown to arise for geometrical reason: they concentrate excess material, allowing the sheet to adopt shapes that cannot be achieved with wrinkles.

Up to know, we do not know how to describe the mechanics of crumples and folds. When they appear, the only way to describe theoretically the morphology of the sheet is to bypass them by using a model where they are not treated explicitly, such as the reduced models described in Sec. 4.1.4.

The geometric model described above can be adapted to elasto-capillary problems if a separation of energy scales is satisfied: if the surface tension (which acts as a load) is too weak to stretch the sheet ($\gamma \ll Y$) but much stronger than bending ($\gamma \gg B/W^2$, where W is the size of the sheet), one just as to minimize the surface energy under the constraint of inextensibility of the sheet and without any cost for bending. Note that when bending is free, compression is allowed for free by wrinkles, crumples or folds. This model can describe satisfactorily the surprising shapes that appear in the Lamé and droplet wrapping experiments [Paulsen et al., 2015, 2017].

4.3 Crumpled sheets

When a sheet is crumpled, a very complex morphology emerges from a very simple loading, confinement in a sphere [Audoly and Pomeau, 2010, Witten, 2007]. The two main questions about crumpling are: what is the resulting morphology? What is it mechanical response? We readily notice that there are stress focuses upon crumpling; as a consequence the plastic limit of the material can be reached easily, leading to a complex force response.

The complexity involved in the description of crumpled paper appears when trying to put together the physical ingredients. In order to describe the morphology, we have to use the equations of elasticity, the Föppl-von Kármán equations, which are non-linear. Another important ingredient for the morphology is self-avoidance: the sheet cannot cross itself. This seemingly simple argument is very difficult to handle in theoretical descriptions; for instance the exact solution for the sheet on liquid problem is not valid after self-contact (Sec. 2.6.2). When self-contact is present, friction matters, which impacts the mechanical response. The mechanical response is also affected by plastic effects; both friction and plasticity forbid to derive the mechanical response from an energy.

First we study two type of stress focusing singularities that may be relevant in crumpled paper: conical and ridge singularities. Then we review briefly what can be done experimentally or numerically.

4.3.1 Conical singularities

The conical singularity, has first been studied theoretically by Ben Amar and Pomeau [1997]. Such shape can easily be obtained experimentally by pushing a sheet through a cylinder with a point force [Chaïeb et al., 1998, Cerda and Mahadevan, 1998].

4.3.1.1 Geometry

In order to describe a conical configuration of the sheet, we choose the polar material coordinates centered at the tip of the cone, where the sheet takes the form [Witten, 2007]

$$\boldsymbol{R}(r,\theta) = r\hat{\boldsymbol{u}}(\theta), \tag{4.86}$$

where $\hat{\boldsymbol{u}}(\theta)$ is a unit vector. The conical shape is completely characterized by its intersection with the unit sphere centered at the tip of the cone, which is given by $\hat{\boldsymbol{u}}(\theta)$.

Provided that $|\hat{\boldsymbol{u}}'(\theta)| = 1$, this configuration is isometric to the planar reference shape. Notably, the Gauss curvature is zero since the sheet is flat in the r-direction, hence the surface is developpable; for this reason, this ideal shape is called the developpable-cone, or just "d-cone". This shape is singular ar $r = 0$, where the curvature vanishes.

In order to get the bending energy, we have to compute the curvature of the sheet at (r,θ) in the θ-direction. Since $\hat{\boldsymbol{u}}(\theta)$ and $\hat{\boldsymbol{u}}'(\theta)$ are orthogonal unit vectors, the normal to the sheet is

$$\hat{\boldsymbol{n}}(\theta) = \hat{\boldsymbol{u}}(\theta) \times \hat{\boldsymbol{u}}'(\theta). \tag{4.87}$$

We note that $\hat{\boldsymbol{u}}(\theta) = \partial_r \boldsymbol{R}(r,\theta)$ and $\hat{\boldsymbol{u}}'(\theta) = r^{-1}\partial_\theta \boldsymbol{R}(r,\theta)$. The curvature in the direction θ is given by

$$c(r,\theta) = \hat{\boldsymbol{n}}(\theta)\cdot r^{-2}\partial_\theta^2 \boldsymbol{R}(r,\theta) = \frac{1}{r}\left[\hat{\boldsymbol{u}}(\theta)\times\hat{\boldsymbol{u}}'(\theta)\right]\cdot \boldsymbol{u}''(\theta) = \frac{\tilde{c}(\theta)}{r}, \tag{4.88}$$

where we have introduced the rescaled curvature $\tilde{c}(\theta)$.

We can parametrize $\hat{\boldsymbol{u}}(\theta)$ in spherical coordinates:

$$\hat{\boldsymbol{u}} = \begin{pmatrix}\cos(\phi)\sin(\beta)\\ \sin(\phi)\sin(\beta)\\ \cos(\beta)\end{pmatrix}, \tag{4.89}$$

where β and ϕ are functions of θ. We can compute

$$\hat{\boldsymbol{u}}' = \phi'\begin{pmatrix}-\sin(\phi)\sin(\beta)\\ \cos(\phi)\sin(\beta)\\ 0\end{pmatrix} + \beta'\begin{pmatrix}\cos(\phi)\cos(\beta)\\ \sin(\phi)\cos(\beta)\\ -\sin(\beta)\end{pmatrix}. \tag{4.90}$$

Notably, the condition $|\hat{\boldsymbol{u}}'| = 1$ reads

$$|\hat{\boldsymbol{u}}'|^2 = \phi'^2\sin(\beta)^2 + \beta'^2 = 1. \tag{4.91}$$

To get simpler and more intuitive expressions, we consider a cone with a small slope: $\beta = \frac{\pi}{2} - \alpha$, with $|\alpha| \ll 1$. We start by rephrasing the isometry condition (4.91). At order α^0, it gives $\phi' = 1$, meaning that $\phi(\theta) = \theta$. We can parametrize the cone using the space coordinate ϕ instead of the material coordinate θ; now the isometry condition is global:

$$2\pi = \int_0^{2\pi}\left[\phi'^2\sin(\beta)^2 + \beta'^2\right]^{1/2}\mathrm{d}\theta = \int_0^{2\pi}\left[\sin(\beta)^2 + \left(\frac{\mathrm{d}\beta}{\mathrm{d}\phi}\right)^2\right]^{1/2}\mathrm{d}\phi \tag{4.92}$$

At order α^2, this relation becomes

$$\int_0^{2\pi}\left[\alpha''(\theta)^2 - \alpha(\theta)^2\right]\mathrm{d}\theta = 0. \tag{4.93}$$

Now the cone is completely defined by the function $\alpha(\phi)$ (the function $\phi(\theta)$ is only a reparametrisation of the unit circle of the original sheet).

We can then compute the curvature as a function of α. At order α, using $\phi = \theta$, we have

$$\hat{\boldsymbol{u}} = \begin{pmatrix}\cos(\theta)\\ \sin(\theta)\\ \alpha\end{pmatrix}, \tag{4.94}$$

$$\hat{\boldsymbol{u}}' = \begin{pmatrix}-\sin(\theta)\\ \cos(\theta)\\ 0\end{pmatrix} + \alpha'\begin{pmatrix}0\\0\\1\end{pmatrix}, \tag{4.95}$$

$$\hat{\boldsymbol{n}} = \hat{\boldsymbol{u}}\times\hat{\boldsymbol{u}}' = \begin{pmatrix}-\alpha\cos(\theta)\\ -\alpha\sin(\theta)\\ 1\end{pmatrix} + \alpha'\begin{pmatrix}\sin(\theta)\\ -\cos(\theta)\\ 0\end{pmatrix}, \tag{4.96}$$

$$\boldsymbol{u}'' = -\begin{pmatrix}\cos(\theta)\\ \sin(\theta)\\ 0\end{pmatrix} + \alpha''\begin{pmatrix}0\\0\\1\end{pmatrix}. \tag{4.97}$$

So that the curvature is

$$\tilde{c}(\theta) = \hat{\boldsymbol{n}}\cdot\boldsymbol{u}'' = \alpha'' + \alpha. \tag{4.98}$$

4.3.1.2 Mechanics

The bending energy of an annular plate $R_c < r < R$ is given by

$$U_{\text{bend}} = \frac{B}{2}\int_{R_{\text{core}}}^{R} r\mathrm{d}r \int_0^{2\pi} \mathrm{d}\theta c(r,\theta)^2 = \frac{B}{2}\log\left(\frac{R}{R_{\text{core}}}\right)\int_0^{2\pi}\tilde{c}(\theta)^2\mathrm{d}\theta. \tag{4.99}$$

The singularity at the tip of the cone appears in the divergence of the bending energy as $R_{\text{core}} \to 0$. In the limit of small slope, the bending energy thus reads

$$U_{\text{bend}} = \frac{B}{2}\log\left(\frac{R}{R_{\text{core}}}\right)\int_0^{2\pi}\left[\alpha''(\theta)+\alpha(\theta)\right]^2\mathrm{d}\theta. \tag{4.100}$$

When a sheet is pushed through a cylinder, a geometrical constraint $\alpha \geq \alpha_0$ is imposed, where α_0 is given by the radius of the cylinder and the indentation depth. To find the shape of the cone, $\alpha(\theta)$, we should minimize the energy (4.100) under the isometry constraint (4.93) and the constraint $\alpha \geq \alpha_0$ (otherwise $\alpha = 0$ would be a solution). This problem resembles Euler buckling, and is also similar to the formation of a ruck in a rug [Vella et al., 2009, Kolinski et al., 2009]. Solving the equations, one gets the angular size of the region that does looses contact with the cylinder: $\Delta\theta \simeq 139°$ [Audoly and Pomeau, 2010].

4.3.1.3 Size of the core

For $r < R_c$, the diverging bending energy is regularized by allowing some stretching. We look for R_c with scaling arguments. The curvature in the isometric region is of order $\tilde{c} \sim \alpha_0$, leading to a bending energy

$$U_{\text{bend}} \sim B\alpha_0^2 \log\left(\frac{R}{R_{\text{core}}}\right). \tag{4.101}$$

The radius of curvature of the core is $R_{\text{curv}} \sim R_{\text{core}}/\alpha_0$, hence its Gauss curvature is $\kappa_G \sim (\alpha_0/R_{\text{core}})^2$, generating a strain $\epsilon \sim \kappa_G R_{\text{core}}^2 \sim \alpha_0^2$ from Eq. (4.18). The stretching energy is thus

$$U_{\text{str}} \sim Y R_{\text{core}}^2 \epsilon^2 \sim Y R_{\text{core}}^2 \alpha_0^2. \tag{4.102}$$

Balancing the bending and stretching energies, we find the optimal value

$$R_{\text{core}} \sim \sqrt{\frac{B}{Y}} \sim t : \tag{4.103}$$

the size of the core should be given by the thickness of the material [Witten, 2007]. The corresponding energy is

$$\boxed{U_{\text{cone}} \sim B\alpha_0^2 \log(R/t).} \tag{4.104}$$

However, the core in much larger in the experiments; it also has a crescent shape, that is to date not completely understood.

4.3.2 Ridge singularities

A ridge appears for instance between two developpable-cones. We denote W the width of the ridge (the distance between the centers of the cones). On the sides of the ridge, a sharp angle α is imposed of the sheet. Having a sharp angle along the ridge would cost an infinite bending energy, so that there

should be a finite curvature radius along the ridge, say $R(s)$, that goes to 0 as $s \to 0$ or $s \to W$. This ridge, which should appear during crumpling, has been studied by Lobkovsky et al. [1995].

We provide a scaling argument for the curvature radius. We just need the maximal curvature radius, $R(W/2) = R$. The bending energy per unit area is

$$U_{\text{bend}} \sim \frac{B}{R^2}. \tag{4.105}$$

The finite radius of curvature generates a stretching ϵ along the ridge, associated to a stretching energy density $U_{\text{str}} \sim Y\epsilon^2$. In order to evaluate ϵ, we consider the maximal deviation ζ of the ridge from a straight line. From geometric arguments we get $\zeta \sim \alpha^2 R$. The stretching of the ridge is $\epsilon \sim (\zeta/W)^2 \sim (\alpha^2 R/W)^2$. The stretching energy density is thus

$$U_{\text{str}} \sim Y \left(\frac{\alpha^2 R}{W}\right)^4. \tag{4.106}$$

Balancing the stretching and bending energies, we find

$$R \sim t^{1/3} W^{2/3} \alpha^{-4/3}. \tag{4.107}$$

The deformation cover an area $W \times \alpha R$, so that the energy of this ridge is

$$\boxed{U_{\text{ridge}} \sim Y t^{5/3} W^{1/3} \alpha^{7/3}.} \tag{4.108}$$

We should note the peculiar scaling of the ridge; one would naively expect a dependence on W and α as $U \sim \alpha^2 W$.

The scaling analysis presented here can be made rigorous by solving the Föppl-von Kármán equations. In this case the scaling results can be derived by a proper rescaling of the equations [Lobkovsky and Witten, 1997].

We compare the energies of cones and ridges. The energy of a ridge (4.108) can be written as $U_{\text{ridge}} \sim B(W/t)^{1/3}\alpha^{7/3}$. For $x = W/t \gg 1$, $x^{1/3} \gg \log(x)$, hence the energy of the ridges should be dominant in a crumpled state.

4.3.3 Experimental and numerical studies

The sheet can be followed in 3D optically during the early stage of crumpling [Aharoni and Sharon, 2010]. At the late stage, the shape can be obtained via X-ray microtomography [Cambou and Menon, 2011]. One can look for instance to the sheet orientation as a function of its position in the crumpled ball, or at the number of contacts, getting information about the role of friction. Another (cheaper) way to get information about the structure is to cut through the crumpled ball [Sultan and Boudaoud, 2006, Deboeuf et al., 2013]. In order to reduce the effect of friction, one can use a fluid in order to lubricate the contacts [Cambou and Menon, 2015].

However, it is not straightforward to reconstruct the shape in material coordinates from the tomography data or from a cut. The properties of the network of ridges may be obtained by analysing the unfolded sheet, plasticity keeping track of the ridges [Blair and Kudrolli, 2005, Sultan and Boudaoud, 2006, Andresen et al., 2007]. From the distribution of ridges length, one can infer that crumpling is hierarchical: long ridges form first, then they break in smaller ridges, and so on, analogously to what happens in repeated folding [Deboeuf et al., 2013]. Moreover, the ridges are not always static, as the conical singularities can move [Aharoni and Sharon, 2010], leaving behind them plastically deformed furrows [Gottesman et al., 2015].

The mechanical response can be obtained by placing the crumpled ball in a cylinder with a weighted piston on it and looking at the displacement of the piston as a function of time (this is a much simpler geometry than a confining sphere with a decreasing radius). Due to the interplay of the hierarchical structure and friction effects, the dynamics may be logarithmic [Matan et al., 2002]: the displacement $h(t)$ follows $h(t) = A \log(t)$ for several decades in time. This dependence is not yet understood. The mechanics can be related to the properties of the sound emitted during crumpling, which is easy to measure [Kramer and Lobkovsky, 1996, Houle and Sethna, 1996].

Finally, numerical simulations allow to choose the ingredients to take into account. For instance, one can simulate the crumpling of non-self-avoiding ("phantom") sheets [Vliegenthart and Gompper, 2006], or tune the effects of plasticity [Tallinen et al., 2009].

Bibliography

Hillel Aharoni and Eran Sharon. Direct observation of the temporal and spatial dynamics during crumpling. *Nat Mater*, 9(12):993–997, 12 2010. ISSN 1476-1122. URL http://dx.doi.org/10.1038/nmat2893. 10.1038/nmat2893.

Christian André Andresen, Alex Hansen, and Jean Schmittbuhl. Ridge network in crumpled paper. *Phys. Rev. E*, 76(2):026108, Aug 2007. doi: 10.1103/PhysRevE.76.026108. URL http://link.aps.org/doi/10.1103/PhysRevE.76.026108.

Shahaf Armon, Efi Efrati, Raz Kupferman, and Eran Sharon. Geometry and Mechanics in the Opening of Chiral Seed Pods. *Science*, 333(6050):1726–1730, 2011. doi: 10.1126/science.1203874. URL http://www.sciencemag.org/content/333/6050/1726.abstract.

B. Audoly. Localized buckling of a floating elastica. *Phys. Rev. E*, 84(1):011605, Jul 2011. doi: 10.1103/PhysRevE.84.011605. URL https://link.aps.org/doi/10.1103/PhysRevE.84.011605.

B. Audoly and Y. Pomeau. *Elasticity and geometry: from hair curls to the non-linear response of shells*. Oxford University Press Oxford, 2010.

M. Ben Amar and Y. Pomeau. Crumpled paper. *Proc. Royal Soc. A*, 453(1959):729–755, 1997. doi: 10.1098/rspa.1997.0041. URL http://rspa.royalsocietypublishing.org/content/453/1959/729.abstract.

Daniel L. Blair and Arshad Kudrolli. Geometry of Crumpled Paper. *Phys. Rev. Lett.*, 94(16):166107, Apr 2005. doi: 10.1103/PhysRevLett.94.166107. URL http://link.aps.org/doi/10.1103/PhysRevLett.94.166107.

Fabian Brau, Hugues Vandeparre, Abbas Sabbah, Christophe Poulard, Arezki Boudaoud, and Pascal Damman. Multiple-length-scale elastic instability mimics parametric resonance of nonlinear oscillators. *Nat Phys*, 7(1):56–60, 01 2011. ISSN 1745-2473. URL http://dx.doi.org/10.1038/nphys1806. 10.1038/nphys1806.

Anne Dominique Cambou and Narayanan Menon. Three-dimensional structure of a sheet crumpled into a ball. *Proceedings of the National Academy of Sciences*, 108(36):14741–14745, 2011. doi: 10.1073/pnas.1019192108. URL http://www.pnas.org/content/108/36/14741.abstract.

Anne Dominique Cambou and Narayanan Menon. Orientational ordering in crumpled elastic sheets. *EPL*, 112(1):14003, 2015. doi: 10.1209/0295-5075/112/14003. URL http://dx.doi.org/10.1209/0295-5075/112/14003.

E. Cerda and L. Mahadevan. Conical Surfaces and Crescent Singularities in Crumpled Sheets. *Phys. Rev. Lett.*, 80(11):2358–2361, Mar 1998. doi: 10.1103/PhysRevLett.80.2358. URL http://link.aps.org/doi/10.1103/PhysRevLett.80.2358.

E. Cerda and L. Mahadevan. Geometry and Physics of Wrinkling. *Phys. Rev. Lett.*, 90(7): 074302, Feb 2003. doi: 10.1103/PhysRevLett.90.074302. URL http://link.aps.org/doi/10.1103/PhysRevLett.90.074302.

Sahraoui Chaïeb, Francisco Melo, and Jean-Christophe Géminard. Experimental Study of Developable Cones. *Phys. Rev. Lett.*, 80(11):2354–2357, Mar 1998. doi: 10.1103/PhysRevLett.80.2354. URL http://link.aps.org/doi/10.1103/PhysRevLett.80.2354.

J. Chopin, V. Démery, and B. Davidovitch. Roadmap to the Morphological Instabilities of a Stretched Twisted Ribbon. *J. Elast.*, 119(1-2):137–189, 2015. ISSN 0374-3535. doi: 10.1007/s10659-014-9498-x. URL http://dx.doi.org/10.1007/s10659-014-9498-x.

Benny Davidovitch, Robert D. Schroll, Dominic Vella, Mokhtar Adda-Bedia, and Enrique A. Cerda. Prototypical model for tensional wrinkling in thin sheets. *Proceedings of the National Academy of Sciences*, 108(45):18227–18232, 2011. doi: 10.1073/pnas.1108553108. URL http://www.pnas.org/content/108/45/18227.abstract.

S. Deboeuf, E. Katzav, A. Boudaoud, D. Bonn, and M. Adda-Bedia. Comparative Study of Crumpling and Folding of Thin Sheets. *Phys. Rev. Lett.*, 110(10):104301, Mar 2013. doi: 10.1103/PhysRevLett.110.104301. URL http://link.aps.org/doi/10.1103/PhysRevLett.110.104301.

Vincent Démery, Benny Davidovitch, and Christian D. Santangelo. Mechanics of large folds in thin interfacial films. *Phys. Rev. E*, 90(4):042401, Oct 2014. doi: 10.1103/PhysRevE.90.042401. URL http://link.aps.org/doi/10.1103/PhysRevE.90.042401.

Haim Diamant and Thomas A. Witten. Compression Induced Folding of a Sheet: An Integrable System. *Phys. Rev. Lett.*, 107(16):164302, Oct 2011. doi: 10.1103/PhysRevLett.107.164302. URL http://link.aps.org/doi/10.1103/PhysRevLett.107.164302.

M. A. Dias, J. A. Hanna, and C. D. Santangelo. Programmed buckling by controlled lateral swelling in a thin elastic sheet. *Phys. Rev. E*, 84(3):036603, Sep 2011. doi: 10.1103/PhysRevE.84.036603. URL http://link.aps.org/doi/10.1103/PhysRevE.84.036603.

J. C. Géminard, R. Bernal, and F. Melo. Wrinkle formations in axi-symmetrically stretched membranes. *The European Physical Journal E*, 15(2):117–126, 2004. ISSN 1292-895X. doi: 10.1140/epje/i2004-10041-1. URL http://dx.doi.org/10.1140/epje/i2004-10041-1.

Omer Gottesman, Efi Efrati, and Shmuel M. Rubinstein. Furrows in the wake of propagating d-cones. *Nature Communications*, 6:7232 EP –, 06 2015. URL http://dx.doi.org/10.1038/ncomms8232. Article.

Paul A. Houle and James P. Sethna. Acoustic emission from crumpling paper. *Phys. Rev. E*, 54 (1):278–283, Jul 1996. doi: 10.1103/PhysRevE.54.278. URL http://link.aps.org/doi/10.1103/PhysRevE.54.278.

Jiangshui Huang, Megan Juszkiewicz, Wim H. de Jeu, Enrique Cerda, Todd Emrick, Narayanan Menon, and Thomas P. Russell. Capillary Wrinkling of Floating Thin Polymer Films. *Science*, 317(5838): 650–653, 2007. doi: 10.1126/science.1144616. URL http://www.sciencemag.org/content/317/5838/650.abstract.

Jiangshui Huang, Benny Davidovitch, Christian D. Santangelo, Thomas P. Russell, and Narayanan Menon. Smooth Cascade of Wrinkles at the Edge of a Floating Elastic Film. *Phys. Rev. Lett.*, 105 (3):038302, Jul 2010. doi: 10.1103/PhysRevLett.105.038302. URL http://link.aps.org/doi/10.1103/PhysRevLett.105.038302.

Jérémy Hure, Benoît Roman, and José Bico. Wrapping an Adhesive Sphere with an Elastic Sheet. *Phys. Rev. Lett.*, 106(17):174301, Apr 2011. doi: 10.1103/PhysRevLett.106.174301. URL https://link.aps.org/doi/10.1103/PhysRevLett.106.174301.

Jungwook Kim, James A. Hanna, Myunghwan Byun, Christian D. Santangelo, and Ryan C. Hayward. Designing Responsive Buckled Surfaces by Halftone Gel Lithography. *Science*, 335(6073):1201–1205, 2012. doi: 10.1126/science.1215309. URL http://www.sciencemag.org/content/335/6073/1201.abstract.

H. King, R. D. Schroll, B. Davidovitch, and N. Menon. Elastic sheet on a liquid drop reveals wrinkling and crumpling as distinct symmetry-breaking instabilities. *Proc. Natl. Acad. Sci. U.S.A.*, 109(25): 9716–9720, 2012. doi: 10.1073/pnas.1201201109.

Yael Klein, Efi Efrati, and Eran Sharon. Shaping of Elastic Sheets by Prescription of Non-Euclidean Metrics. *Science*, 315(5815):1116–1120, 2007. doi: 10.1126/science.1135994. URL http://www.sciencemag.org/content/315/5815/1116.abstract.

John M. Kolinski, Pascale Aussillous, and L. Mahadevan. Shape and Motion of a Ruck in a Rug. *Phys. Rev. Lett.*, 103(17):174302, Oct 2009. doi: 10.1103/PhysRevLett.103.174302. URL http://link.aps.org/doi/10.1103/PhysRevLett.103.174302.

Eric M. Kramer and Alexander E. Lobkovsky. Universal power law in the noise from a crumpled elastic sheet. *Phys. Rev. E*, 53(2):1465–1469, Feb 1996. doi: 10.1103/PhysRevE.53.1465. URL http://link.aps.org/doi/10.1103/PhysRevE.53.1465.

Alex Lobkovsky, Sharon Gentges, Hao Li, David Morse, and Thomas A. Witten. Scaling properties of stretching ridges in a crumpled elastic sheet. *SCIENCE-NEW YORK THEN WASHINGTON-*, pages 1482–1484, 1995.

Alexander E. Lobkovsky and T. A. Witten. Properties of ridges in elastic membranes. *Phys. Rev. E*, 55(2):1577–1589, Feb 1997. doi: 10.1103/PhysRevE.55.1577. URL http://link.aps.org/doi/10.1103/PhysRevE.55.1577.

C. Majidi and R. S. Fearing. Adhesion of an elastic plate to a sphere. *Proceedings of the Royal Society A: Mathematical, Physical and Engineering Sciences*, 464(2093):1309–1317, 2008. doi: {10.1098/rspa.2007.0341}URL.

M. Marder, E. Sharon, S. Smith, and B. Roman. Theory of edges of leaves. *Europhysics Letters (EPL)*, 62(4):498–504, may 2003. doi: 10.1209/epl/i2003-00334-5. URL https://doi.org/10.1209%2Fepl%2Fi2003-00334-5.

Kittiwit Matan, Rachel B. Williams, Thomas A. Witten, and Sidney R. Nagel. Crumpling a Thin Sheet. *Phys. Rev. Lett.*, 88(7):076101, Jan 2002. doi: 10.1103/PhysRevLett.88.076101. URL http://link.aps.org/doi/10.1103/PhysRevLett.88.076101.

J. D. Paulsen, V. Démery, C. D. Santangelo, T. P. Russell, B. Davidovitch, and N. Menon. Optimal wrapping of liquid droplets with ultrathin sheets. *Nat Mater*, 14(12):1206–1209, 12 2015. ISSN 1476-1122. URL http://dx.doi.org/10.1038/nmat4397. Letter.

J. D. Paulsen, V. Démery, K. B. Toga, Z. Qiu, T. P. Russell, B. Davidovitch, and N. Menon. Geometry-Driven Folding of a Floating Annular Sheet. *Phys. Rev. Lett.*, 118(4):048004, Jan 2017. doi: 10.1103/PhysRevLett.118.048004. URL http://link.aps.org/doi/10.1103/PhysRevLett.118.048004.

Joseph D. Paulsen, Evan Hohlfeld, Hunter King, Jiangshui Huang, Zhanlong Qiu, Thomas P. Russell, Narayanan Menon, Dominic Vella, and Benny Davidovitch. Curvature-induced stiffness and the spatial variation of wavelength in wrinkled sheets. *Proceedings of the National Academy of Sciences*, 113(5):1144–1149, 2016. doi: 10.1073/pnas.1521520113. URL http://www.pnas.org/content/113/5/1144.abstract.

William H. Paulsen. What is the shape of a Mylar balloon? *American Mathematical Monthly*, pages 953–958, 1994.

Miguel Piñeirua, Nana Tanaka, Benoit Roman, and Jose Bico. Capillary buckling of a floating annulus. *Soft Matter*, 9(46):10985–10992, 2013. doi: 10.1039/C3SM51825F. URL http://dx.doi.org/10.1039/C3SM51825F.

L. Pocivavsek, R. Dellsy, A. Kern, S. Johnson, B. Lin, K. Y. C. Lee, and E. Cerda. Stress and Fold Localization in Thin Elastic Membranes. *Science*, 320(5878):912–916, 2008. doi: 10.1126/science.1154069.

Charlotte Py, Paul Reverdy, Lionel Doppler, José Bico, Benoît Roman, and Charles N. Baroud. Capillary Origami: Spontaneous Wrapping of a Droplet with an Elastic Sheet. *Phys. Rev. Lett.*, 98 (15):156103, Apr 2007. doi: 10.1103/PhysRevLett.98.156103. URL http://link.aps.org/doi/10.1103/PhysRevLett.98.156103.

B. Roman and J. Bico. Elasto-capillarity: deforming an elastic structure with a liquid droplet. *Journal Of Physics-Condensed Matter*, 22(49):493101, 2010. doi: 10.1088/0953-8984/22/49/493101. URL http://stacks.iop.org/0953-8984/22/i=49/a=493101.

H. S. Seung and David R. Nelson. Defects in flexible membranes with crystalline order. *Phys. Rev. A*, 38(2):1005–1018, Jul 1988. doi: 10.1103/PhysRevA.38.1005. URL http://link.aps.org/doi/10.1103/PhysRevA.38.1005.

Eran Sharon and Efi Efrati. The mechanics of non-Euclidean plates. *Soft Matter*, 6(22):5693–5704, 2010. doi: 10.1039/C0SM00479K. URL http://dx.doi.org/10.1039/C0SM00479K.

Eran Sharon, Benoit Roman, Michael Marder, Gyu-Seung Shin, and Harry L. Swinney. Mechanics: Buckling cascades in free sheets. *Nature*, 419(6907):579–579, 10 2002. ISSN 0028-0836. URL http://dx.doi.org/10.1038/419579a. 10.1038/419579a.

Eran Sharon, Benoît Roman, and Harry L. Swinney. Geometrically driven wrinkling observed in free plastic sheets and leaves. *Phys. Rev. E*, 75(4):046211, Apr 2007. doi: 10.1103/PhysRevE.75.046211. URL https://link.aps.org/doi/10.1103/PhysRevE.75.046211.

Robert W. Style, Rostislav Boltyanskiy, Yonglu Che, J. S. Wettlaufer, Larry A. Wilen, and Eric R. Dufresne. Universal Deformation of Soft Substrates Near a Contact Line and the Direct Measurement of Solid Surface Stresses. *Phys. Rev. Lett.*, 110(6):066103, Feb 2013. doi: 10.1103/PhysRevLett.110.066103. URL http://link.aps.org/doi/10.1103/PhysRevLett.110.066103.

Eric Sultan and Arezki Boudaoud. Statistics of Crumpled Paper. *Phys. Rev. Lett.*, 96(13):136103, Apr 2006. doi: 10.1103/PhysRevLett.96.136103. URL http://link.aps.org/doi/10.1103/PhysRevLett.96.136103.

T. Tallinen, J. A. Astrom, and J. Timonen. The effect of plasticity in crumpling of thin sheets. *Nat Mater*, 8(1):25–29, 01 2009. ISSN 1476-1122. URL http://dx.doi.org/10.1038/nmat2343. 10.1038/nmat2343.

G Taylor. On the shape of parachutes. *Advisory Committee for Aeronautics*, 1919.

Hugues Vandeparre, Miguel Piñeirua, Fabian Brau, Benoit Roman, José Bico, Cyprien Gay, Wenzhong Bao, Chun Ning Lau, Pedro M. Reis, and Pascal Damman. Wrinkling Hierarchy in Constrained Thin Sheets from Suspended Graphene to Curtains. *Phys. Rev. Lett.*, 106(22):224301, Jun 2011. doi: 10.1103/PhysRevLett.106.224301. URL http://link.aps.org/doi/10.1103/PhysRevLett.106.224301.

D. Vella, P. Aussillous, and L. Mahadevan. Elasticity of an interfacial particle raft. *EPL (Europhysics Letters)*, 68(2):212, 2004. URL http://stacks.iop.org/0295-5075/68/i=2/a=212.

Dominic Vella, Arezki Boudaoud, and Mokhtar Adda-Bedia. Statics and Inertial Dynamics of a Ruck in a Rug. *Phys. Rev. Lett.*, 103(17):174301, Oct 2009. doi: 10.1103/PhysRevLett.103.174301. URL http://link.aps.org/doi/10.1103/PhysRevLett.103.174301.

Dominic Vella, Amin Ajdari, Ashkan Vaziri, and Arezki Boudaoud. Wrinkling of Pressurized Elastic Shells. *Phys. Rev. Lett.*, 107(17):174301, Oct 2011. doi: 10.1103/PhysRevLett.107.174301. URL https://link.aps.org/doi/10.1103/PhysRevLett.107.174301.

G. A. Vliegenthart and G. Gompper. Forced crumpling of self-avoiding elastic sheets. *Nat Mater*, 5(3):216–221, 03 2006. ISSN 1476-1122. URL http://dx.doi.org/10.1038/nmat1581. 10.1038/nmat1581.

T. A. Witten. Stress focusing in elastic sheets. *Rev. Mod. Phys.*, 79(2):643–675, Apr 2007. doi: 10.1103/RevModPhys.79.643. URL http://link.aps.org/doi/10.1103/RevModPhys.79.643.